The influence of the solar wind dynamic pressure and of the B_Z component of the interplanetary magnetic field on the magnetic storm index

A Thesis Submitted to the
College of Graduate Studies and Research
in Partial Fulfillment of the Requirements
for the degree of Master of Science
in the Department of Physics and Engineering Physics
University of Saskatchewan
Saskatoon

By

MD. MAHAMUDUL HASAN CHOWDHURY

Permission to Use

In presenting this thesis in partial fulfillment of the requirements for a Postgraduate degree from the University of Saskatchewan, I agree that the Libraries of this University may make it freely available for inspection. I further agree that permission for copying of this thesis in any manner, in whole or in part, for scholarly purposes may be granted by the professor or professors who supervised my thesis work or, in their absence, by the Head of the Department or the Dean of the College in which my thesis work was done. It is understood that any copying or publication or use of this thesis or parts thereof for financial gain shall not be allowed without my written permission. It is also understood that due recognition shall be given to me and to the University of Saskatchewan in any scholarly use which may be made of any material in my thesis.

Requests for permission to copy or to make other use of material in this thesis in whole or part should be addressed to:

Head of the Department of Physics and Engineering Physics
163 Physics Building
116 Science Place
University of Saskatchewan
Saskatoon, Saskatchewan
Canada
S7N 5E2

Abstract

The solar wind has an important impact on the Earth and its magnetic field. Among the solar wind perturbations, there can be jumps in the solar wind dynamic pressure as well as strong magnetic excursions in the z-component of the Interplanetary Magnetic Field (IMF B_Z). When coronal mass ejections and other solar disturbances take place in the solar wind, there can be clear changes in the global geomagnetic field, as measured by a magnetic index called Sym-H. In this thesis some unusual events were found for which there were large fluctuations either in the solar wind dynamic pressure or in the IMF B_Z but not simultaneously in both. These events suggest that the response of the geomagnetic field to the dynamic pressure fluctuations of the solar wind is variable. In particular, it was found that the earthward component (x-component) of the IMF appeared to influence the magnitude of the Sym-H response. By contrast, there was no visible impact of the y-component of the IMF. In a second exceptional event it was found that the IMF was changing substantially while the solar wind dynamic pressure remained very constant. From this study a time delay between the IMF B_Z component and the resulting Sym-H was found to be of the order of 60 to 90 minutes.

Acknowledgements

At first I would like to thank and show my deepest gratitude to my supervisor, Dr. Jean-Pierre St-Maurice, who guided me and gave me tremendous support throughout this degree. He gave me the opportunity to come to the University of Saskatchewan and work with him. His encouragement, advice and boundless patience on me helped me to complete my degree successfully. I am blessed that I had the opportunity to work with him and got him as my supervisor. I am grateful to all of the SuperDARN group members for sharing their knowledge. Thanks to Dr. Pasha Ponomarenko and to all my student colleagues for their unconditional support and for the help they provided when I needed it. I thank the NSF for funding me to attend the 2012 ISR Summer School. I thank NASA GSFCs Space Physics Data Facility's OMNIWeb, SuperDARN and the World Data Center for Geomagnetism, Kyoto for their data, which were very vital to this work. Special thanks to all Bangladeshi students, studying at the U of S, for supporting me in my bad times and given me the feeling of living in a family.

Thanks to the Almighty for having given me the opportunity to get another masters degree. Thanks to my parents for their valuable advice and the mental support they have provided from thousands kilometers away.

.

Contents

List of Tables

List of Figures

List of Abbreviations

CIR	Corotating Interaction Region
CME	Coronal Mass Ejection
Dst	Disturbed Storm Time
FAC	Field Aligned Current
GSM	Geocentric Solar Magnetospheric System
HF	High Frequency
IMF	Interplanetary Magnetic Field
IR	Interaction Region
MLT	Magnetic Local Time
RC	Ring Current
Re	Radius of the Earth
SC	Sudden Commencement
SI	Sudden Impulse
SOHO	Solar and Heliospheric Observatory
SQ	Solar quiet
SSC	Storm Sudden Commencement
SuperDARN	Super Dual Auroral Radar Network
Sym-H	Symmetric H-component (of the geomagnetic field)
UT	Universal Tim

CHAPTER ONE

INTRODUCTION

This thesis deals with the interaction of the solar wind with the Earth's magnetosphere. The Sun and the Earth represent a coupled dynamic system. The space between the Earth and the Sun is filled with the solar wind plasma. This solar wind also carries with it a magnetic field, which allows it to interact strongly with the Earth's magnetosphere. The interaction of the solar wind magnetic field with the Earth's magnetosphere has a great effect on the near-Earth space environment. The effect of this interaction is called space weather. Space weather is an important topic of current research. Space weather can pose a danger to trans-polar flights, while geomagnetically induced current can flow through power lines and pipelines near the surface and damage them as a result of auroral disturbances. Extreme space weather situations are called geomagnetic storms, and are defined as periods of intense geomagnetic activity. Geomagnetic activity is primarily driven by magnetic reconnection between the Interplanetary Magnetic Field (IMF) and the terrestrial magnetic field. As the dipole of the Earth magnetic field is close to perpendicular to the ecliptic plane, geomagnetic activity primarily depends on the southward component of the IMF (*Vasyliunas, 1975*). Coherent solar wind structures containing southward magnetic fields and high velocities are most efficient drivers of space weather events.

We can observe the geomagnetic activity with ground-based magnetometers. Geomagnetic storms have been related to the interaction of the solar wind with the Earth's magnetosphere. The solar wind dynamic pressure pulses and the southward interplanetary magnetic field are two

major key factors that change the magnetic field of the Earth through changes in the magnetospheric current system. Due to the solar wind dynamic pressure, the dayside magnetosphere is compressed. The resulting increase in magnetopause current thus increases the geomagnetic field. A strongly southward-directed interplanetary magnetic field enhances the ring current, which is an equatorial westward current flow around the Earth due to particle drift. The link with a southward IMF is less direct than with pressure pulses. At first the plasma from the Earth merges with the solar wind plasma. The Earth plasma is then dragged by the solar wind to the night side. Reconnection in the magnetotail then injects plasma back towards the Earth. This plasma feeds the ring currents as the ions are deflected westward (and electrons eastward) by the magnetic field gradient. The resulting changes in the ring currents can be monitored through magnetic indices like Dst, Sym-H, AP and Kp. The changes in the geomagnetic activity affect the ionospheric motion, which can be monitored by the SuperDARN HF radars through the production of convection maps.

The goal of this thesis is to analyze the interaction of the solar wind dynamic pressure with the Earth's magnetosphere and see how the solar wind dynamic pressure, the interplanetary magnetic field (particularly the z-component) and the Sym-H behave under certain conditions.

In Chapter 2, I discuss the basic principles needed for this thesis. This includes the properties of the sun, the solar wind, the interplanetary magnetic field and the Earth's magnetospheric field. Chapter 3 deals with a brief discussion on the data sets and their origin. In Chapter 4 events selection is discussed. Chapter 5 deals with the data analysis.

CHAPTER TWO

BACKGROUND

2.1 The Sun and solar wind:

The Sun's atmosphere consists of three layers: the photosphere, the chromosphere and the corona. The lowest layer is the photosphere, which is thin, and emits most of the Sun's light. At the bottom of the photosphere the temperature is 6600 K and at the top it is 4300 K (*Priest, 1997*). The chromosphere lies above the photosphere. The average particle density of this region is $10^{17}\ m^{-3}$ and the temperature is 10^6 K (*Priest, 1997*). The region beyond the chromosphere is called the corona. This layer extends radially outwards into the interplanetary space beyond the solar system. This extremely hot layer temperature reaches almost double the temperature of the chromosphere. Each layer of the Sun's atmosphere is quite different. The photosphere reveals the granulated structure of the convection zone. We also see sunspots on the solar surface. Sunspots consist of a dark cool central region surrounded by a penumbra and they appear typically in pairs with a leading sunspot and trailing sunspot.

The Sun is magnetically active with an 11-year cycle of activity. During one 11-year cycle it reverses its magnetic field polarity. A full cycle is roughly 22 years in duration with two magnetic reversals. A full solar cycle is known as the Hale cycle. Sunspots have been used to monitor the Sun's activity level due to their high visibility. During the 11-year cycle the sunspots number reaches a maximum before dropping to a minimum. Solar cycle 23, which was very strong, began in May 1996 and ended in December 2008. During solar maximum, solar

phenomena such as sunspots are seen in the photosphere. Solar prominences, solar flares, coronal mass ejections, and corotating interaction regions are also common. During this time the Sun is considered ‘active’.

The Sun’s magnetic field emerges from the photosphere. It has a very complicated and dynamic structure and consists of looping field lines connecting from one umbra to another. The Sun’s magnetic field comes out from one hemisphere, extends into interplanetary space, and then comes back to the opposite hemisphere. The magnetic field lines above and below the equatorial plane are therefore in opposite directions.

When the solar wind comes into contact with the Earth’s magnetic field the shape of the Earth’s magnetic field changes. The solar wind is the dominant force on the outer surface of the magnetosphere. The solar wind is a supersonic flow of ionized plasma and magnetic field that goes through the interplanetary medium. The solar wind mainly consists of electrons and protons and very small amounts of ionized helium and heavy ions. The magnetic pressure difference between the solar corona and interplanetary space drives the solar flow in opposite to solar gravity. The solar wind is highly conductive and, due to this, a magnetic field is frozen into the solar wind plasma and travels with it through interplanetary space. The solar wind is often a highly structured plasma stream, which is going radially out of the corona at supersonic speeds [*Brueckner and Bartoe, 1983*]. The mean velocity of the inner corona particles is about 145km/s, which is much lower than the solar escape velocity (618 km/s). Still many particles achieve enough energy to reach a velocity of 400 km/s by 1 AU. These particles feed the solar wind. At the temperature of the Sun’s corona, electrons, due to their small mass, reach escape velocity and build up an electric field, which accelerates ions away from the Sun.

Because of the presence of the solar wind the Sun's extended magnetic field takes a unique twisted shape, called the Parker spiral. When the magnetic field comes out of the Sun's immediate vicinity it is called the Interplanetary Magnetic Field (IMF). The spiral pattern of the magnetic field is shown in Figure 2.1. In this figure the observer is looking down at the equatorial plane of the Sun. The solid lines indicate the IMF structure with the Sun at the center. The outflowing solar wind and rotating solar surface creates the spiral shape. The IMF structure of the Sun is divided into two different sectors; the sunward going field lines (blue) and the field lines going away from the Sun (red). Green solid lines indicate ''sector boundaries''.

2.2 Coronal Mass Ejection:

Sometimes a massive burst of high-energy plasma emerges from the solar corona into the interplanetary space. This eruption of high-energy plasma is called Coronal Mass Ejection (CME). Most CMEs originate from the active regions of the Sun's surface (*Cliver and Ling, 2001*). The frequency of CME's depends on the solar cycle. Most of the CMEs occur during solar maximum, when sunspots are most prevalent, [*Cliver and Ling, 2001; Webb and Howard, 1994; Alves et al, 2006*]. A CME can consists of billions of tons of plasma and have a strong magnetic field [*Webb and Howard, 1994; Temmer et. al., 2010*]. According to the standard model [*Webb and Howard, 1994*] a CME originates from an expanding solar prominence in the corona. A recent study suggests that the phenomenon of magnetic reconnection on the Sun is responsible for CME [*Temmer et. al. 2010*]. According to the *Temmer et. al.* study, a significant amount of energy stored in the magnetic fields is transferred to plasma particles. The particles then accelerate along newly closed magnetic field lines into the lower chromosphere. Magnetic

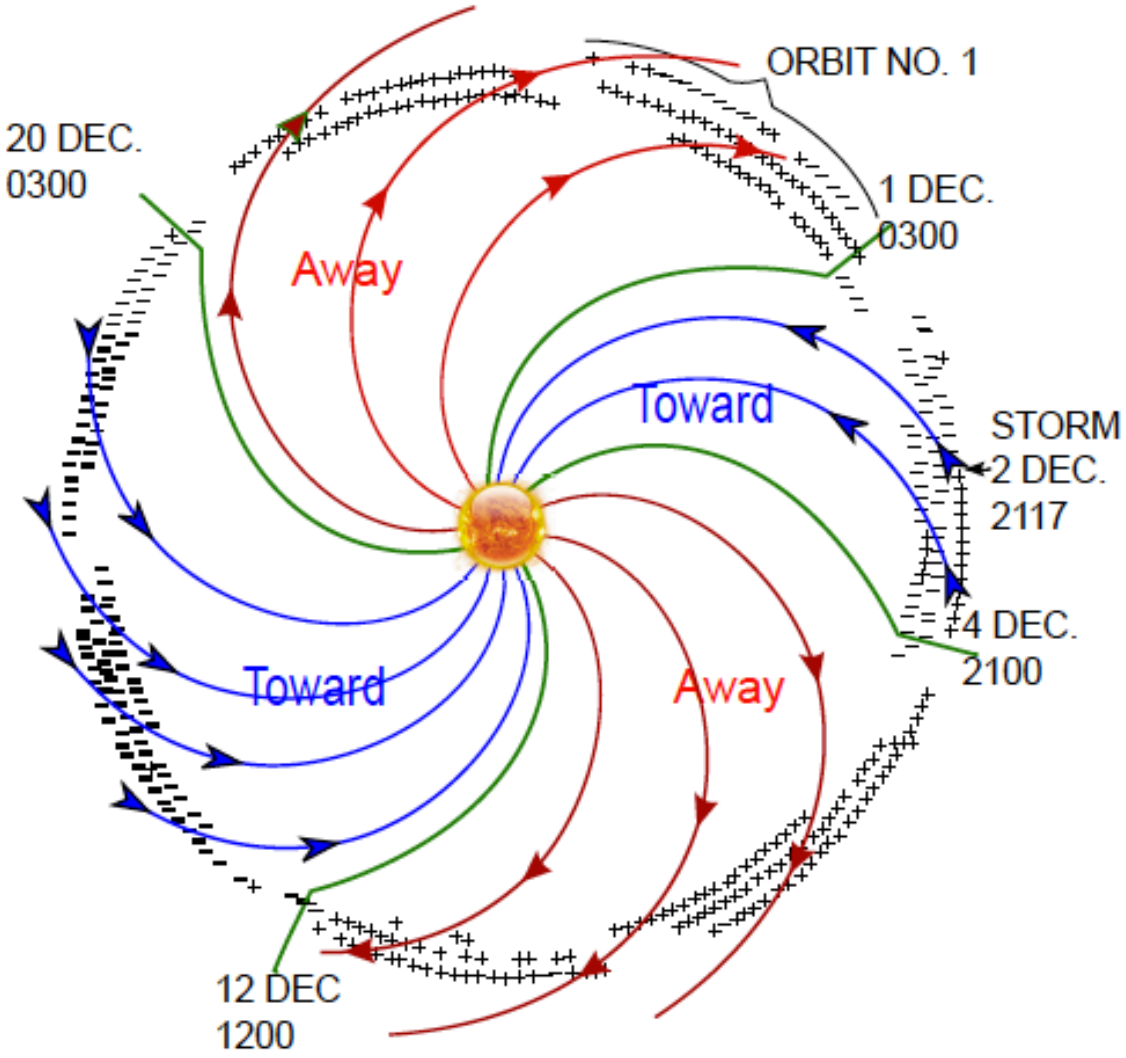

Figure 2.1: Solar sector boundary crossing and Parker spiral [taken from *Wilcox 1966*]. Magnetic field lines are shown in blue (towards the Sun) and red (away from the Sun). Sector crossings are outlined in green. Positive signs and negative signs are the polarity of the magnetic field lines.

reconnection may happen on solar arcades—a series of closely occurring loops of magnetic lines of force. These lines of force quickly reconnect into a low arcade of loops, leaving a helix of magnetic field unconnected to the rest of the arcade. The sudden release of energy in this reconnection causes a solar flare. The unconnected magnetic helical field and the material it contains may violently expand outwards, forming a CME. This also explains why CMEs and solar flares typically erupt from the active regions of the Sun where magnetic fields are much stronger. When a CME is directed towards the Earth, it's called 'halo' CME. At a distance of 1AU from the Sun it was measured that during solar cycle 23 the CME plasma ranges in speed from 500 km/s to 2700 km/s [*Zhang et al., 2007*]. A typical coronal mass ejection may have any or all of the three distinctive features: a cavity of low electron density, a dense core (the prominence, which appears as a bright region on coronagraph images embedded in this cavity), and a bright leading edge [*Illing and Hundhausen, 1983; Tokman and Bellan, 2002*].

2.3 Corotating Interaction Region:

As mentioned earlier, sunspots, flares, prominences, and CMEs occur more frequently near solar maximum. During solar minimum coronal holes are the more active phenomenon. Coronal holes are regions of low density ($5\times10^{11}\mathrm{m}^{-3}$) and temperatures ($1.6\times10^{6}$ K) of the Sun compared to the surrounding medium (*Priest, 1997*). Coronal holes form at lower latitudes as a result of CMEs (*Richardson, 2004*) and are the primary source of the high-speed component of the solar wind plasma, having average speeds of 800 km/sec (*Heber et al., 1999; Priest, 1997; Alves, 2006*). This 'fast' solar wind flows radially outward from the coronal hole. When the fast solar wind catches up with the slower solar wind, the density and thermal energy of the plasma of the

fast solar wind increases in the region where the fast solar wind catches up with the slow solar wind (*Alves et al., 2006*). The interaction regions where the fast solar wind catches up with the slow solar wind are called stream interface. Intuitively it can be seen that these interaction regions will have a spiral shape that may wrap multiple times around the Sun. These regions are called "co-rotating interaction regions" or CIRs since they co-rotate with the Sun.

The solar wind interaction described above is displayed in Figure 2.2. In the figure the Sun is at the bottom and the solid line around it represents the Earth's orbit.

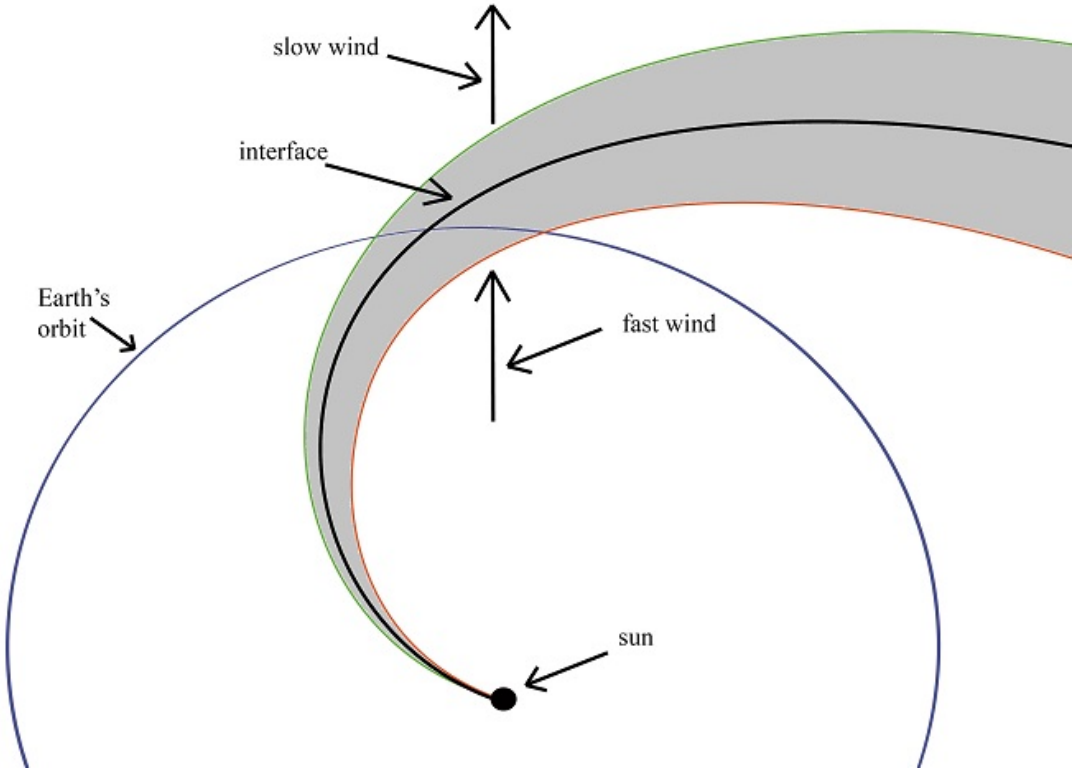

Figure 2.2: An idealized CIR stream in the equatorial plane. Image adapted from *Borovsky and Denton, 2010*.

2.4 Magnetosphere:

A magnetosphere is a cavity in the solar wind flow formed by the interaction of the solar wind and the interplanetary magnetic field with the intrinsic magnetic field or ionized upper atmosphere of a planetary body (*Southwood and Kivelson, 2001*). The Earth is surrounded by a magnetosphere. By the presence of its magnetosphere the Earth is largely shielded from the influence of the solar wind. The shape of the magnetosphere is influenced by the drag of the solar wind and this drag is predominantly caused by a mechanism known as reconnection. When reconnection occurs the magnetic field of the solar wind makes contact with the magnetic field of the magnetosphere. The factors that control reconnection are not completely understood but a southern direction of the interplanetary field is critical to enabling the reconnection with the dayside.

The position of the magnetospheric boundary, particularly up front, is determined by the balance between the solar wind dynamic pressure and the pressure exerted by the magnetosphere, principally that of its magnetic field. The effect of the solar wind and its IMF on the magnetosphere cavity is illustrated in Figure 2.3. The incoming solar wind compresses the magnetosphere on the sunward side. The magnetic field lines are lengthened on the night side creating the magnetotail region.

As the solar wind approaches the Earth, it encounters the geomagnetic field. It is possible to determine the approximate location of the magnetopause boundary by considering the pressure balance between the geomagnetic field and the solar wind. The approximate dynamic pressure of the solar wind is given by

$$P_{dyn} = \frac{1}{2}\rho_{sw}u_{sw}^2 \qquad 2.1$$

where $\rho_{sw}$and u_{sw} are the proton mass density and flow speed respectively. By balancing the solar wind dynamic pressure with the magnetic pressure of the geomagnetic field the approximate location of the dayside boundary is determined by (*Walker and Russel 1997*):

$$L_{mp}(R_e) = 107.4(n_{sw}u_{sw}^2)^{-1/6}. \qquad 2.2$$

Typically this distance is around 10 Re (Earth radii) upstream of the Earth but under strong solar wind driving the magnetopause can be pushed well inside geostationary orbit (at 6.6 Re where a satellite orbiting around the Earth has a 24-hour rotation period and thus remains at a constant longitude above the Earth). In the antisunward direction, the solar wind flow deforms the dipolar magnetic field to a cometary tail-like shape where the magnetopause is on average about 30 Re from the Sun-Earth line, depending on the solar wind pressure. The magnetotail extends far beyond the lunar orbit, that is, at least a few hundred Re in the antisunward direction. As the solar wind flows past the magnetosphere, it is both supersonic and super-Alfvénic. As a result, a bow shock is formed upstream of the magnetopause, and the flow is decelerated within the magnetosheath between the bow shock and the magnetopause.

The Earth's internal field, the solar wind plasma and the interplanetary magnetic field determine the size and shape of the magnetosphere. The response of the magnetosphere varies with the changes in the dynamic pressure of the solar wind and the orientation of the interplanetary magnetic field. When the orientation of the interplanetary magnetic field and the Earth's magnetic field lines are antiparallel, merging occurs on the dayside and reconnection occurs on

the night side and energy and momentum are easily transferred from the solar wind to the magnetosphere.

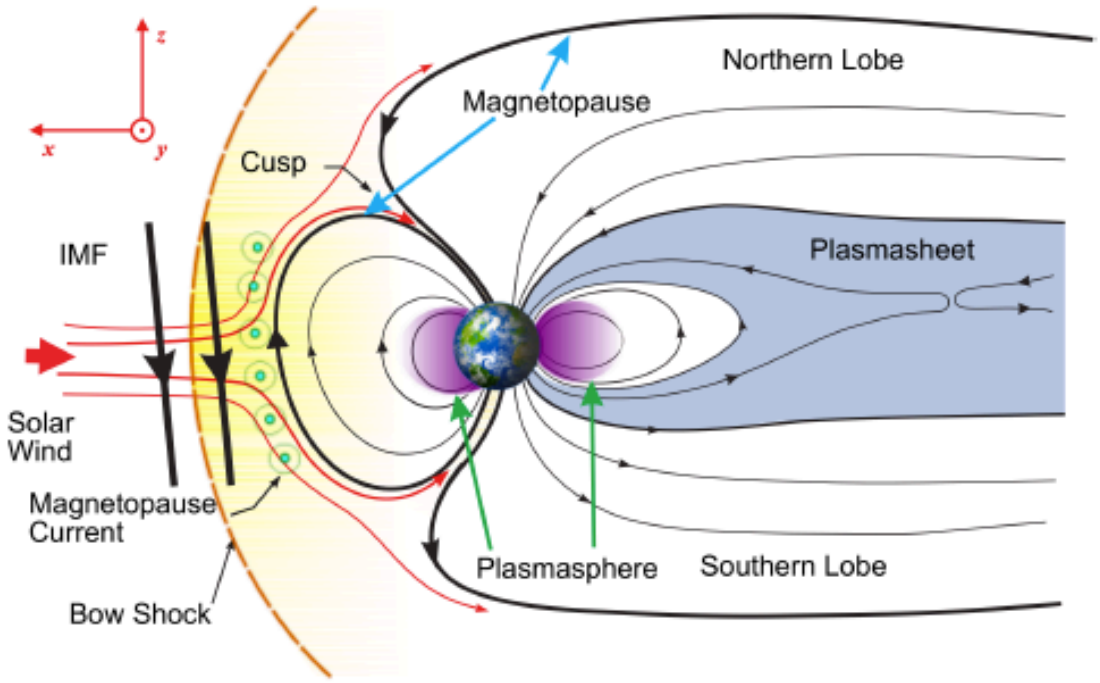

Figure 2.3: Interaction of the solar wind with the magnetosphere. Various Magnetospheric and current systems are labelled with the GSM coordinate system. Taken from *Megan Gillies* thesis with her permission.

2.5 Magnetospheric Currents

The solar wind carries a magnetic field with it and if this field is anti-parallel to the Earth's field the magnetic field lines attract and recombine. This is the ''reconnection'' or ''merging''

process. It takes place whenever there are 2 antiparallel magnetic fields, for example one southward (solar wind) and one northward (earth). As solar particles move into the field of the Earth they create an equatorial current known as the Chapman Ferraro current. This current is caused by the deflection of electrons and ions in the opposite direction in the magnetopause. The Chapman-Ferraro current is shown in Figure 2.4. The magnetic field strength of the near-equatorial dayside magnetopause is twice as great as the dipole field of the Earth at that location. This is because the dipole field is canceled by the magnetopause current outside the magnetopause and at the same time such as to create an equal but opposite field just inside the magnetopause. This field adds to the dipole field of the Earth and doubles it in the vicinity of the magnetopause.

Note that the magnetopause currents move around the equator and need to be closed. They therefore begin to move around the magnetosheath back to the dawn-side. This also enhances the effects of currents in the equatorial plane of the tail, resulting in two loops of current (solenoids), one clockwise, one counter-clockwise. These solenoids create magnetic fields away from and toward the earth, elongating the tail (Figure 2.5).

The reconnection alluded to in a previous paragraph allows solar wind plasma to be linked to the magnetosphere and move magnetospheric plasma across the Earth's poles. When plasma flows across the poles it experiences a **V**x**B** force. This separates the positive charge to the dawn side and electrons to the dusk side creating an electric field. Now consider the tail events; as the plasma from the sun flows past the Earth, magnetic field lines are moved close to one another near the magneto-tail, causing reconnection events. When reconnection occurs in the tail, plasma particles of solar wind origin get trapped in the magnetosphere and bounce back and forth between the north and south magnetic poles of the Earth's magnetic field lines.

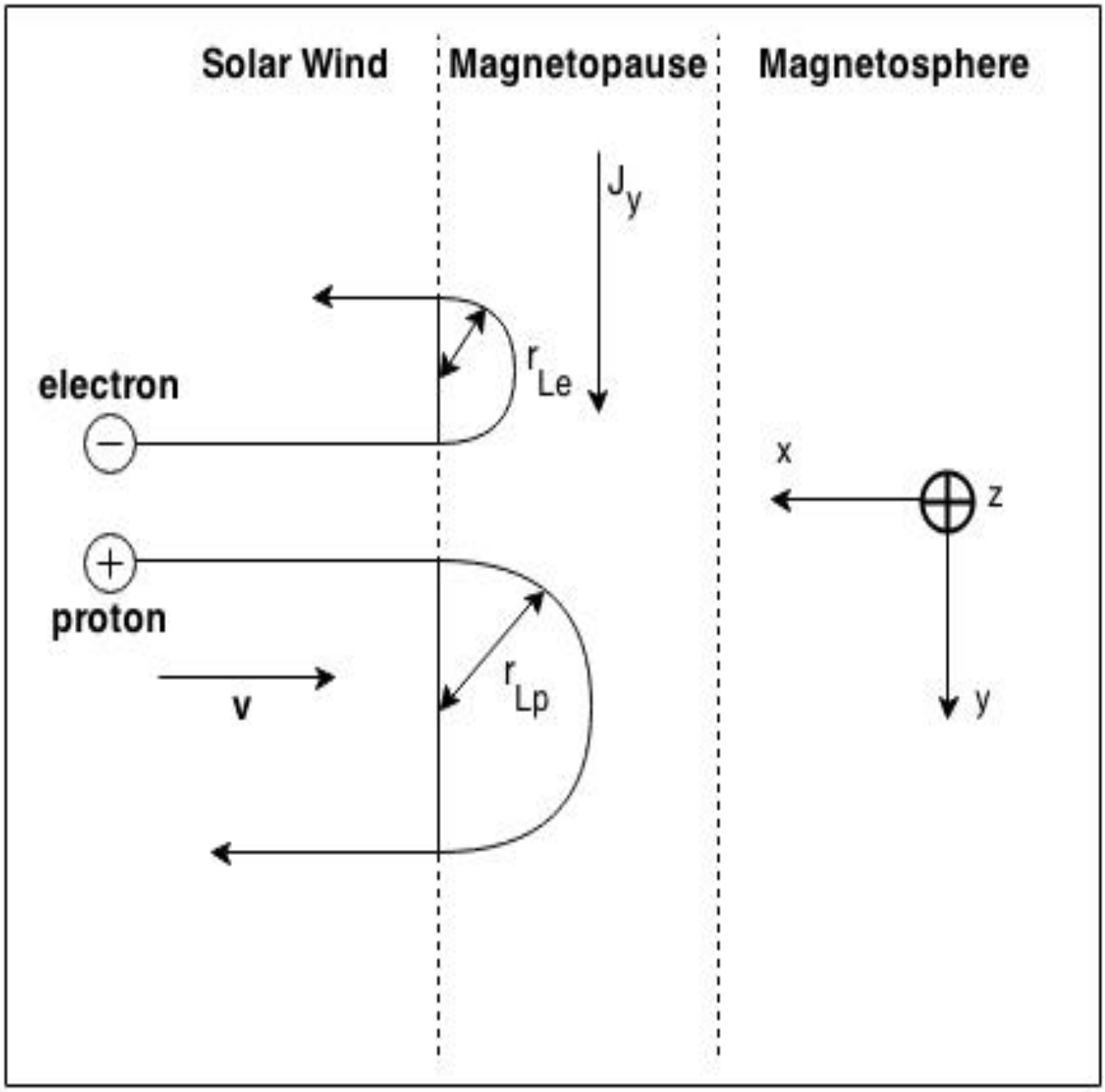

Figure 2.4: Magnetopause current system as viewed from the equatorial plane. The Sun is located in the negative-X direction and the Earth in the positive-X direction. Image adapted from *Hughes, 1997.*

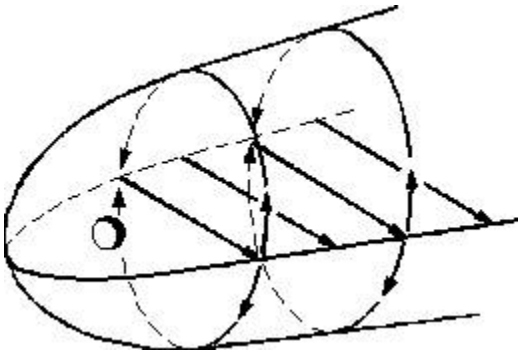

Figure 2.5: Tail side currents caused by closing of the Chapman currents (solenoid effect). Image taken from *http://www.phy6.org/Educatcc/Sconct17.htm*

The magnetic field gradient causes the ions and electrons to undergo curvature gradient drift (Baunjohann *and Treumann, 2006*). Due to curvature gradient drift, the ions flow to the dusk side and the electron flow to the dawn side and generate a westward current circling the earth. This current is known as the ring current. The ring current itself produces a magnetic field, which modifies the Earth's equatorial magnetic field, particularly the horizontal component. With time, the ring currents lose their extra charges through precipitation into the atmosphere, where they produce the aurora.

2.6 Magnetospheric Convection:

As described in the previous section, a southward solar wind magnetic field forces the plasma to flow over the polar regions. As a result, the ionosphere flows from local noon to local midnight, in the polar regions, corresponding to the magnetospheric flow of the open field lines from the dayside magnetopause to the magnetotail. After magnetotail reconnection in the distant tail, plasma particles are accelerated back toward the Earth.

The resulting ionospheric image of the magnetospheric flow at the north pole of the Earth is illustrated in Figure 2.6 in cartoon form. It shows twin flow vortices associated open field lines that flow away from the Sun over the polar cap and closed field lines that flow toward the Sun at lower latitudes.

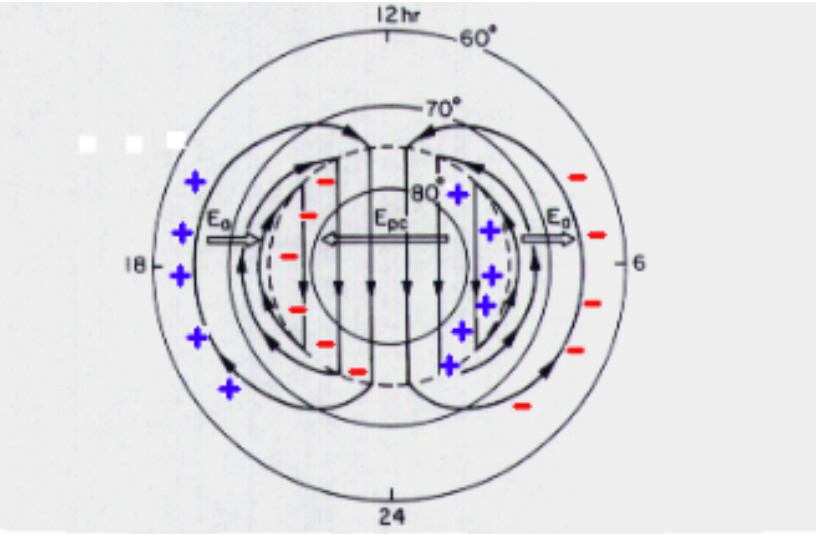

Figure 2.6: Ionospheric image of the plasma flow over high latitude. Field-aligned currents originating in the magnetosphere produce the charges. Image adopted from schematic by Jean-Pierre St Maurice.

2.7 Ionospheric Currents:

The ionosphere is coupled to the magnetosphere by highly structured and dynamic field-aligned currents (FAC). Field-aligned currents are an integral part of magnetosphere-ionosphere coupling (*Cowley, 2000*). Figure 2.7 illustrates the direction and location of the FAC currents while Figure 2.6 showed the resulting regions of charges in the ionosphere. The currents are going into and out of the ionosphere during both quiet and disturbed geomagnetic activity levels.

Region 1 currents are directed downward on the dawn side and upward on the dusk side. The currents equatorward of Region 1 are known as Region 2 currents (*Iijima and Potemra, 1978*). They are directed downward on the dusk side and upward on the dawn side. The regions where current flows upward of the ionosphere are negatively charged regions and where currents flow into the ionosphere are positively charged region. This creates a dawn–to-dusk electric field at the polar cap region and dusk-to-dawn electric field at equatorward latitudes (Figure 2.6).

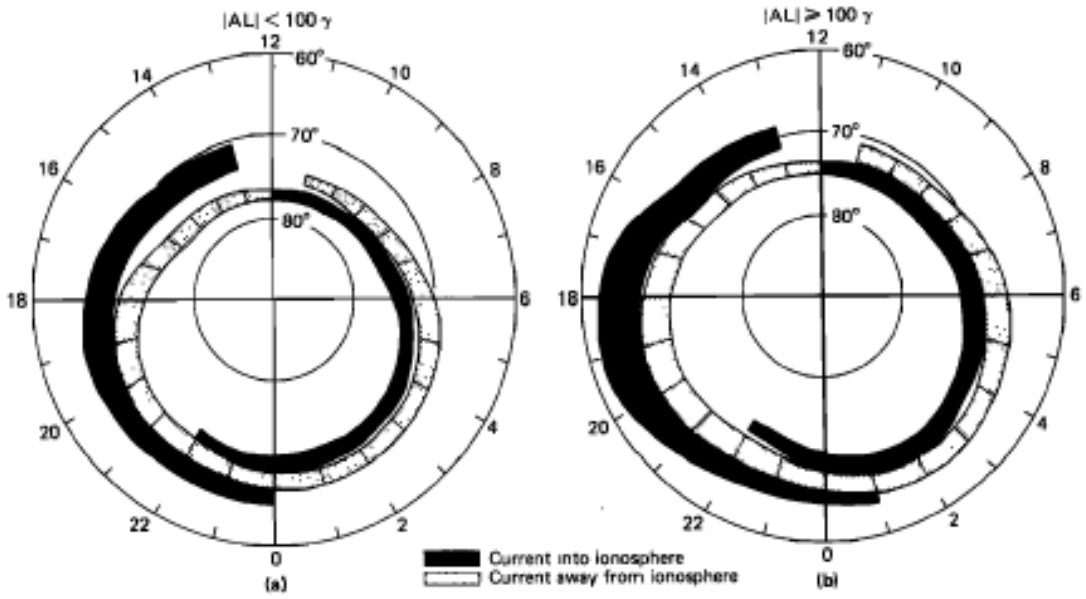

Figure 2.7: Field-aligned Current pattern showing Region 1 and Region 2 currents for both quiet (left) and disturbed (right) geomagnetic conditions (*Iijima and Potemra, 1978*).

In the ionosphere the motion of the electrons and ions is strongly related to the ratio of the collision frequency to the gyrofrequency (*Kelly, 1989*). Above 100 km the gyrofrequency (a frequency of rotation of a charged particle proportional to its charge and field and inversely

proportional to mass of the particle) of the electron is greater than the collision frequency and thus acquires a drift motion. Above 120 km the ions drift with electron with an **E**x**B** motion**.** The ion-neutral collision frequency increases with the decrease of the altitude below 120 km. Due to collision of the ions with neutrals, ions become free from the magnetic field and the drift with a component of motion along the **E** direction. In the F region, the ions and electrons are highly magnetized because they have a greater gyrofrequency than the collision frequency. Then the general motion of the ions and electrons becomes

$$\boldsymbol{V}_E = \frac{\mathbf{E}\times\mathbf{B}}{\mathrm{B}^2}$$

where $\boldsymbol{V}_E$ is also known as the **E**×**B** drift.

The relative motion of the ions and electrons at different altitudes creates a current system in the E region. The various motions of the ions and electrons and their associated current are shown in Figure 2.8 where the magnetic field is in the z-direction and the electric field in the y-direction. In Figure 2.8 the motion of the ions and electrons are shown at different altitude (100 km, 120 km, 160 km). At 100 km, repeated collisions result in the ions having a small velocity component of v along the y-axis (along **E**) and the electrons in the direction of $\boldsymbol{V}_E$. This creates a current nearly opposite the **E**×**B** drift. Between 110 and 150 km, collisions with the neutrals enable the ions to move in a direction other than the $\boldsymbol{V}_E$direction. This results in a current with a component along the **E** and the **E**×**B** directions. The component of the current moving parallel to the electric field is called the Pedersen current. The component moving perpendicular to both the magnetic and electric fields is called the Hall current. The Hall current flows in a direction perpendicular to both the electric and the magnetic fields, and forms a closed current loop inside the ionosphere. The Pedersen currents, on the other hand, flow in the direction of **E** and therefore must close outside of the ionosphere (illustrated in Figure 2.9).

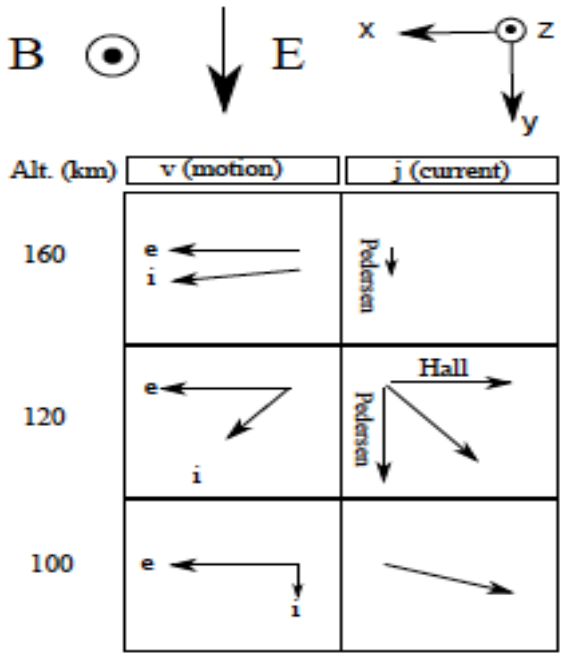

Figure 2.8: Cartoon of ion and electron motion, and resulting ionospheric currents, as a function of altitude.

2.8 Geomagnetic Activity:

As discussed before, the dynamic pressure of the solar wind and the strength and orientation of the interplanetary magnetic field control the magnetospheric and ionospheric current system. Any changes within these parameters will change the magnetosphere-ionosphere current system and will create a variation in the magnetic field observed near the ground of the Earth. This is known as geomagnetic activity. There are some indices to monitor the geomagnetic activity such as Dst (or Sym-H), Ap, Kp. Geomagnetic activity indices are rather well correlated with events of the Sun. The Sun exerts its influence through the solar wind. There is much less magnetic activity if the interplanetary magnetic field, embedded by the solar wind, is not antiparallel to the Earth's magnetic field near the subsolar point on the dayside magnetopause. When the interplanetary magnetic field turns southward, energy flow from the solar wind to the magnetosphere increases and storms and substorms, period of enhanced geomagnetic activity on

a global scale (*Akasofu and Chapman, 1963a, b; Perreault and Akasofu, 1978*), occur in the magnetosphere and ionosphere. Magnetospheric substorms are the most frequent type of geomagnetic activity.

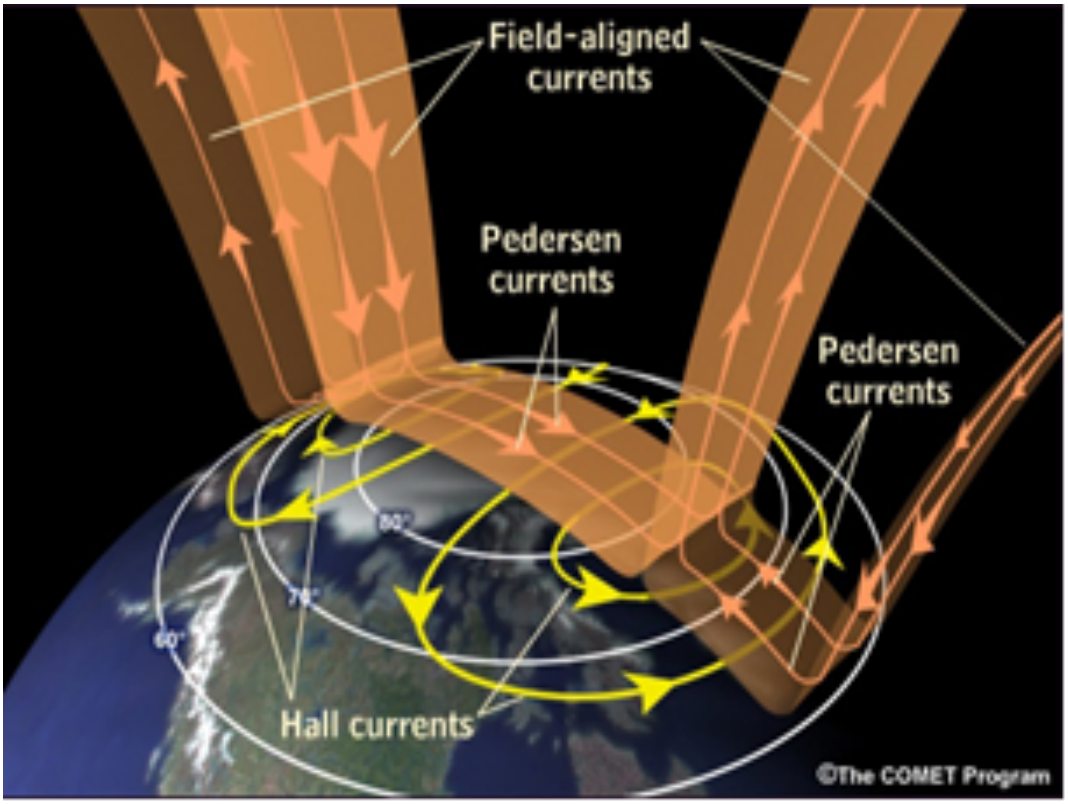

Figure 2.9: Global representation of the ionospheric Hall current and Pedersen current system coupled to the FAC current system as viewed from above. [Image source: MetED, https: //www.meted.ucar.edu/index.php).

When the coupling of the solar wind to the magnetosphere becomes strong and prolonged, geomagnetic activity becomes intense and magnetic storms occur. As a result, the magnetic field of the Earth changes. The ground stations monitor the changes and measure the changes by

hourly average 'Disturbance Storm-Time' (Dst) index and its one-minute counterpart Symmetric H-component (Sym-H) index (*Wanliss and Showalter, 2006*). The Dst index and the Sym-H index are widely used to monitor geomagnetic storms. In this study Sym-H index is being used instead of Dst because of its one-minute resolution. A storm sometimes begins with a sudden increase in the geomagnetic field strength, which is the initial phase of the geomagnetic storm. The magnetopause current induced by an increase in dynamic pressure produces this initial phase. The initial phase is followed by the main phase of the geomagnetic storm. At the main phase of a storm the Dst index drops to sharply negative values reaching as much as of few hundreds nTs. The main phase is followed by a recovery phase that can last from several hours to several days. During recovery phase, Dst begins to recover and gradually returns to its normal pre-storm value. The size of a geomagnetic storm is classified as moderate (-50 nT >minimum of Dst > -100 nT), intense (-100 nT > minimum Dst > -250 nT) or super-storm (minimum of Dst < -250 nT). A typical storm lasts for 1-5 days.

CHAPTER THREE

DATA SETS AND DATA ANALYSIS TECHNIQUE

Three data sets are used in this study of geomagnetic storms from both an interplanetary and an Earth based view point. In this thesis the Symmetric-H (Sym-H) index has been used instead of the Dst because of its higher temporal resolution. The ionospheric convection velocities during storms were measured by using SuperDARN. To identify the solar wind and the IMF features, the Operating Mission as Nodes on the Internet (OMNI) (*http://nssdc.gsfc.nasa.gov/omniweb*) web based database was used.

3.1 Solar wind and IMF observation:

The interplanetary data were obtained from the OMNI database (*http://nssdc.gsfc.nasa.gov/omniweb*). The database provides key parameters such as the interplanetary magnetic Field (IMF), and the solar wind proton velocity time-shifted approximately to the nose of the bow shock. The time-shifted IMF and solar wind data are available for public access through the Space Physics Data Facility website (http://cdaweb.gsfc.nasa.gov/istp-public/). The data provided by OMNI have been processed using the so-called phase front propagation technique of *Weimer et al. (2003)* and *Weimer (2004)* that time shifts the spacecraft data to 17 Re upstream of earth. This proves better for a comparison between upstream solar wind and IMF measurements and geomagnetic observations. The data presented here were used to study the solar wind and IMF parameters taken from the

WIND satellite. The WIND satellite orbit is at the L1 Lagrangian position. The key parameters chosen for the thesis are IMF components, solar wind flow speed, Sym-H and the solar wind dynamic pressure (calculated using the solar wind flow speed and density).

3.2 Ground-Based Magnetic sensing:

Magnetometers measure the geomagnetic field in a localized area. Chains of magnetometers enable the observation of the ionospheric or magnetospheric current system by recording the changes in the geomagnetic field strength. As discussed in Chapter 2, the current can be greatly affected by the fluctuations in the solar wind and IMF. To determine whether the measured geomagnetic activity comes from a localized disruption (like an electrojet) or a global change (like the ring current) it is useful to understand where the global magnetic field strength comes from. An index represents the average of globally placed magnetometers of similar latitudes and a localized region of geomagnetic activity will not substantially affect that index. A common tool to monitor the large-scale changes in the geomagnetic field is at mid latitudes with the Dst index, although for the higher temporal resolution needed in the present work, the Sym-H index has been used.

3.3 The Disturbed Storm Time Index:

The Dst or disturbance storm time index is a measure of geomagnetic activity used to assess the severity of magnetic storms. It is expressed in nanoteslas (nT) and is based on the average value

of the horizontal component of the Earth's magnetic field measured hourly at four low latitude geomagnetic observatories away from regions of ionospheric currents like the auroral and equatorial electrojets. The location of the observatories outlined in Table 3.1.

Dst Observatory	Geographic Longitude(degree)	Geographic Latitude(degree)
Hermanus	19.22	-34.40
Honolulu	201.98	21.32
Kakioka	140.18	36.23
San Juan	293.88	18.11

Table 3.1: Magnetic observatory locations used to calculate the global magnetic activity Dst index.

From the five magnetically 'quietest' days of the year the annual baseline H-component is calculated. An hourly change in the H-component is then calculated by subtracting the baseline value from the average value observed by a given observatory during that hour.

$$\Delta H(t) = H_{obs} - H_{base}(t) \qquad (3.1)$$

The solar quiet time current (SQ) is a prominent feature in quiet geomagnetic conditions. This SQ current is generated by tidal motion. It is necessary to remove the perturbation of the geomagnetic field of the SQ current from the data for each observatory. By removing the SQ

variation from the observed change in the H-component the disturbance variation, $D(t)$ is calculated.

$$D(t) = \Delta H(t) - S_q(t) \qquad (3.2).$$

Then to calculate the Dst value the mean value D (t) of the four contributing observatories is normalized to the magnetic dipole equator

$$D_{st}(t) = \sum_{i=1}^{i=4} \frac{D_i(t)}{\cos(\emptyset_i)} \qquad (3.3)$$

where $\emptyset_i$ is the latitude.

Use of the Dst as an index of storm strength is possible because the strength of the surface magnetic field at low latitudes is inversely proportional to the energy content of the ring current, which increases during geomagnetic storms. In the case of a classic magnetic storm, the Dst often shows a sudden rise, corresponding to the storm sudden commencement in association with an increase in dynamic pressure, and then decreases sharply as the ring current intensifies. Once the IMF turns northward again and the ring current begins to recover, the Dst begins a slow rise back to its quiet time level.

3.4 The Symmetric H-component index:

Sym-H index is a higher resolution (1 minute) H-component profile (*Wanliss and Showalter, 2006*). Sym-H is more useful for the present work because of its higher resolution (*Menvielle et*

al., 2011). The geographic and magnetic coordinates of the six mid-latitude magnetometers which are used to calculate Sym-H are listed in the table 3.2.

Observatory	Geographic		Magnetic	
	Lat. (degree, N)	Long (degree, E)	Lat. (degree, N)	Long (degree, E)
Fredericksburg	38.20	282.630	48.40	353.38
Tucson	32.17	249.27	39.88	316.11
Memambetsu	43.91	144.189	35.35	211.26
Urumqi	43.80	87.7	34.34	162.53
Hermanus	-34.40	19.22	-33.98	84.02
Honolulu	21.32	202.00	21.64	269.74

Table 3.2: Magnetic Observatory locations used in the calculation of the global magnetic activity Sym-H index.

The derivation of Sym-H component is almost the same as Dst. The main difference between Dst and Sym-H is their temporal resolution. Rapid variations in solar wind dynamic pressure, interplanetary magnetic field or the effect of substorm onset are more clearly seen in the Sym-H than the hourly Dst index. Aside from this, Dst uses 4 magnetometers where Sym-H uses 6 and the Sym-H index uses a dipole co-ordinate system.

3.5 SuperDARN HF Radars:

SuperDARN radar is a primary tool to study ionospheric convection (*Greenwald et al., 1995; Chisham et al., 2001*). SuperDARN monitors the mid to high latitude ionosphere and provides

ionospheric convection maps of the northern hemisphere and southern hemisphere.SuperDARN is a high frequency coherent scatter radar which operates in the 8-20 MHz range. It provides high latitude **E**x**B** ionospheric plasma convection. Each of the SuperDARN radars has a field of view consisting of 16 scanned beams. Their positions are separated in azimuth by around 3.24 degrees which gives a full field of view of 52 degrees. There are usually 75 range gates in every beam and each range gate is 45 km in extent. The first range gate is 180 km from the radar site. There are 4 more antennas either ahead or behind of the main antennas to determine the elevation angle of arrival of the returned signal. Depending on the scan mode the standard dwell time for each beam is 3 seconds or 7 seconds. The ionospheric signal occurs from the scattering of radio waves originating from ionospheric irregularities aligned with geomagnetic field lines. The received information is then converted into an auto correlation function (ACF) from which it is possible to determine various parameters such as Doppler shift, spectral width and back scattered power. An estimate of the line-of-sight (l-o-s) velocity can be measured from the Doppler shift of the received data. By processing the l-o-s velocity data a global convection pattern is then produced for every one or two minutes (*Baker and Wing, 1989; Ruohoniemi and Baker, 1998*)

Ionized plasma in the ionosphere propagates perpendicularly to the geomagnetic field lines. The geomagnetic lines are almost vertical at the E and F region of the high latitude ionosphere. In order to receive back the transmitted SuperDARN radio waves to its receiver the radio wave needs to be refracted perpendicularly to the magnetic field lines. The SuperDARN radars receive this signal at 8-20 MHz because at this frequency the radio waves refract enough in the ionosphere to approach the irregularities perpendicularly to the geomagnetic field. These irregularities drift at the **E**x**B** plasma velocity at the F region heights. SuperDARN provides a global view of convection patterns and structures. Sometimes there are some missing data.

That's because of either lack of irregularities or propagation effects. The geographic and geomagnetic co-ordinates of the northern hemisphere SuperDARN radars are given in the table 3.3.

Radar Station	Geographic co-ordinate(in degree)		Geomagnetic co-ordinate(in degree)	
	latitude	longitude	latitude	longitude
Goose Bay	53.32N	60.46W	61.94N	23.02E
Kapuskasing	49.39N	82.32W	60.06N	N 9.22W
Saskatoon	52.16N	106.53W	61.34N	45.26W
Prince George	53.98N	122.59W	59.88N	65.67W
Kodiak	57.60N	152.2W	57.17N	96.28W
Pykkvibaer	63.86N	19.20W	64.59N	69.65E
Hankasalmi	62.32N	26.61E	59.78N	105.53E
King Salmon	58.68N	156.65W	57.43N	100.51E
Wallops Island	37.93N	75.47W	30.63N	75.52E
Hokkaido	43.53N	143.61E	38.14N	145.67W
Inuvik	68.42N	133.5W	72.96N	28.17W
Rankin Inlet	62.82N	93.11W	72.97N	28.17W

Table 3.3: Geographic and geomagnetic co-ordinates of the northern hemisphere SuperDARN radars

The goal of the present thesis is to establish the connection between the solar wind properties (primarily the solar wind dynamic pressure and IMF) and the currents that it triggered on a global scale and can be monitored through the Sym-H index.

CHAPTER FOUR

EVENT SELECTION

The characteristics of the Earth's magnetosphere and Ionosphere depend mostly on the properties of the solar wind. Any change in the properties of the solar wind will produce a wide range of consequences in the Earth's magnetosphere and ionosphere. Changes in the solar wind dynamic pressure and in the orientation and strength of the interplanetary magnetic field are the best-known triggers. A sudden change in solar wind dynamic pressure produces a sudden change in the magnetic field value. Changes in the orientation and strength of the interplanetary magnetic field influence the development of geomagnetic storms or substorms. Geomagnetic storms or substorms are related to the interaction of the magnetosphere with solar wind. A strong southward interplanetary magnetic field produces a geomagnetic storm or substorm but generally a northward interplanetary magnetic field does not (*Akasofu and Chapman, 1963; Gonzalez et al., 1994, 1999*). Geomagnetic storms are discussed in terms of geomagnetic activity. The geomagnetic activity increases in response to large increases in the magnetospheric and ionospheric current system, which can be monitored by ground-based magnetometers. Solar wind dynamic pressure pulses and the southward component of the IMF are the key factors able to change the magnetospheric current system. The magnetopause current varies with the variation of the solar wind dynamic pressure and strongly southward IMF reconnection increases the ring currents at the tail of the magnetosphere.

A magnetic storm can have three phases: the initial phase, the main phase and the recovery phase (*Perreault and Akasofu, 1978*). The initial phase, which is not always present, is caused by the

intensification of the magnetopause currents produced by the arrival of elevated solar wind dynamic pressure. Next, a steady decrease of Dst is seen in the main phase. The decrease in the Dst occurs when plasma is injected into the inner magnetosphere from the magnetotail, which increases the ring currents. After reaching a minimum the Dst starts to recover slowly. In the recovery phase Dst returns to its pre-storm level. In our study we preferred to use Sym-H, to indicate the strength of symmetric H component, over the Dst because of the higher temporal resolution of the former.

As we discussed earlier it is normal to expect to have the dynamic pressure of the solar wind and the z-component of the interplanetary magnetic field both change simultaneously in storms and substorms. It is hard to find events where any one of them does not change. In the current study we searched for events where any one of the two factors remains unchanged. *Gillies et al (2012)* first selected a list of magnetic storms and studied the response of the Sym-H and the circulation in the Earth plasma (through SuperDARN). They showed that anytime they had a storm, there was a close connection between the minimum reached by the IMF B_Z and the minimum reached in the Sym-H index one to two hours later. They also showed that a sudden change in Sym-H is closely related to a sudden change in solar wind dynamic pressure. The present study was approached from the other direction by looking first for events where there was a jump in the dynamic pressure of the solar wind or in the IMF. We then looked at the response of the Sym-H as well as the response of the plasma circulation. The question was to check if, in other words, all changes in dynamic pressure led to simultaneous changes in the Sym-H and if all the negative excursions in the northward IMF component lead to well defined storms.

Physically, and as discussed in Chapter 1, a sudden increase in the solar wind dynamic pressure compresses the dayside of the magnetosphere until the plasma pressure in the magnetosheath

matches with the pressure in the magnetosphere (*Shue et al., 1997*). One obvious question that can also be asked is: if there is a sudden decrease in the solar wind dynamic pressure, is there also a sudden decrease in the Sym-H index? One objective was therefore to look for events where there was a drastic change in the dynamic pressure of the solar wind and observe the consequences on the Sym-H and in the SuperDARN convection map.

4.1 Events Selection

To start to look for events we choose 1998 as our reference year. The reason of selecting this year is that this was a relatively active year from the solar point of view. Figure. 4.1 shows how this study selected the various events. In a normal case, Sym-H changes in response to a change in the solar wind dynamic pressure and in the interplanetary magnetic field. In attempting to isolate the two effects, at first we looked for events where there would be sudden change in solar wind dynamic pressure. We then looked at interplanetary magnetic field. Figure 4.1 shows a sample of data for the IMF z-component, Sym-H, and dynamic pressure on May 1998. The data were taken from the WIND satellite. The top row is for the z-component of the IMF, the middle row is for the solar wind dynamic pressure and the bottom row is for Sym-H. There are a few peaks in the dynamic pressure, which are above 10 nPa. Sym-H also has few peaks. These peaks appear to be related to the dynamic pressure. However, the IMF z-component also changes at the same time. Figure 4.1 displays a full month of data. It is clearly hard to differentiate the influence of the solar wind dynamic pressure and interplanetary magnetic field on this kind of scale. To separate the effect of solar wind dynamic pressure and interplanetary magnetic field we

had to pick the various peaks of Sym-H, solar wind dynamic pressure and interplanetary magnetic field and analyze them

We got lots of events resembling Figure 4.1, where all the solar wind parameters are changing at the same time. These are not useful events for a study where we wanted to isolate dynamic pressure effects from IMF B_Z effects. For this study we searched for events where those two controlling parameters behave independently of each other. However such events proved to be hard to find. We ended up categorizing the observations into three groups: (1) solar wind dynamic pressure changes with time without IMF B_Z changes, (2) IMF B_Z changes without solar wind dynamic pressure changes and (3) both parameters (IMF and solar wind dynamic pressure) changing together.

4.1.1 Case I: solar wind dynamic pressure changes without IMF (B_Z) changes:

Figure 4.2 describes a time period in which the IMF B_Z remained constant for several hours while the solar wind dynamic pressure changed a lot. This was a rare event. After getting this event we took a closer look at the relationship between the Sym-H and the solar wind dynamic pressure and found a relation between the change of dynamic pressure and the change of Sym-H as a function of some other variable. However the time scale was large and by dealing with only one event, it seemed difficult to predict exactly the magnitude of the Sym-H response as a function of dynamic pressure. At the beginning of the time period, the Sym-H was around -70 nT and the dynamic pressure around 5 nT. Then the magnitude of Sym-H started to decrease and the solar wind dynamic pressure slightly gradually increased. Five hours later the Sym-H reached a minimum and then underwent a sharp fall, following the fall in the dynamic pressure. Sym-H

continued to fall and reached its minimum value of -70 nT. Twelve hours later the dynamic pressure went through a sudden increase. A steep change in Sym-H followed the sudden change

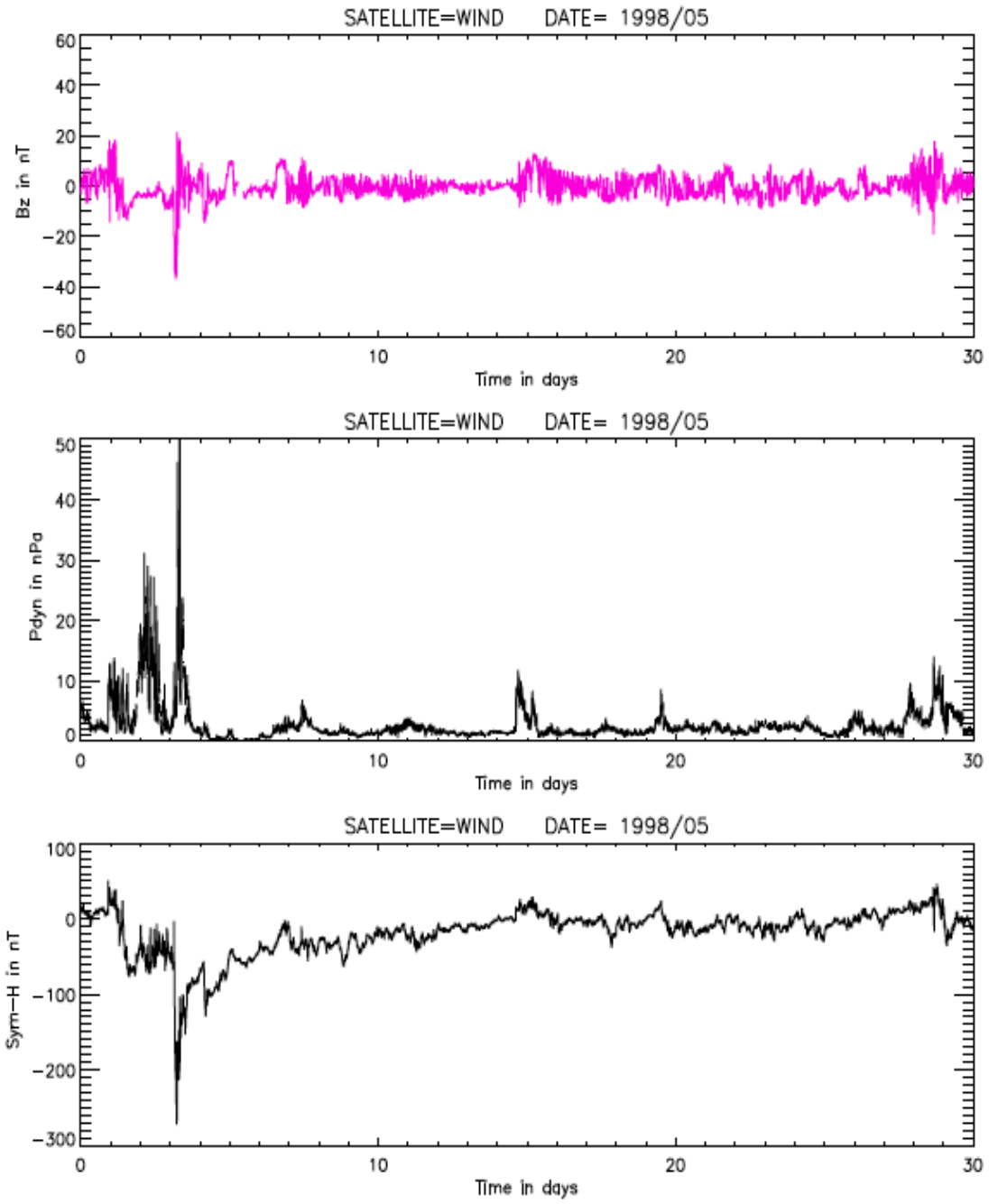

Figure 4.1: Sample of the IMF z-component, Sym-H and solar wind dynamic pressure data on May 1998.

in dynamic pressure. That gives a strong indication that the solar wind dynamic pressure and the Sym-H are related to each other as expected from the processes discussed in Chapter 1 (larger dynamic pressure triggering stronger boundary currents at the magnetopause, so as to increase the overall magnetic field of the Earth). One intriguing fact, however, is that the magnitude of the response seems to vary a lot with time. This motivated taking a look at the other parameters in the solar wind properties. In particular, we studied the other components of the IMF, namely the IMF B_Y and B_X values. Though the IMF B_Z was not absolutely constant, the change was slight and appeared small enough to be ignored.

4.1.2 Case II: IMF changes without solar wind dynamic pressure changes

This study uncovers another rare example. This case is the opposite of the first case. In that case the dynamic pressure was constant while the IMF B_Z changed significantly. The time period for this case is from 00 UT on 5th May 1998 to 12 UT on 5th May 1998. In Figure 4.3 the IMF B_Z starts with a positive value and Sym-H starts with a large negative value. After two and half hours the IMF B_Z goes negative by 20 nT. After a few minutes of the transition of the IMF the Sym-H goes through a large fall and maintains large negative values for the rest of the time period. This phenomenon is unlike what was presented by *Gillies et al* (2012) where it was shown that sudden falls in Sym-H were usually accompanied by changes in the solar wind dynamic pressure for typically a couple of hours. But in the present case there is no change in the dynamic pressure and the Sym-H definitely follows B_Z. *Gillies et al.* (2012) found that Sym-H typically goes to its negative peak value 90 minutes after B_Z goes to its negative peak. To study how Sym-H responds to the IMF B_Z when the solar wind dynamic pressure is almost constant, scatter plots of Sym-H versus B_Z for different time lags were produced. Those plots will be discussed in Chapter 5.

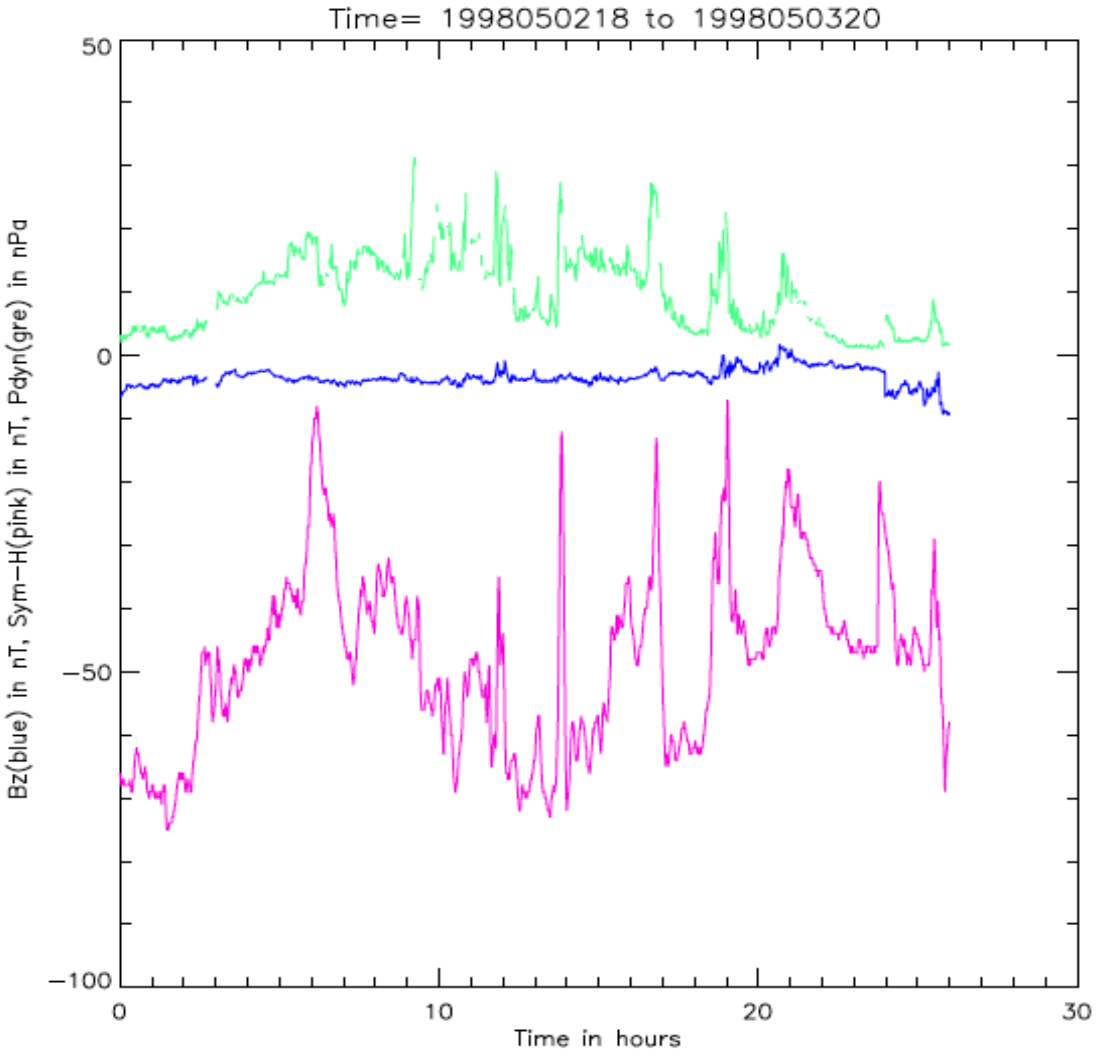

Figure 4.2: Fluctuations of Sym-H (pink) and of the dynamic pressure of the solar wind (green) and the IMF Z-component (blue) with time. The starting time is 18 UT on 2nd May of 1998 and the ending time is 20 UT on 3rd May of 1998.

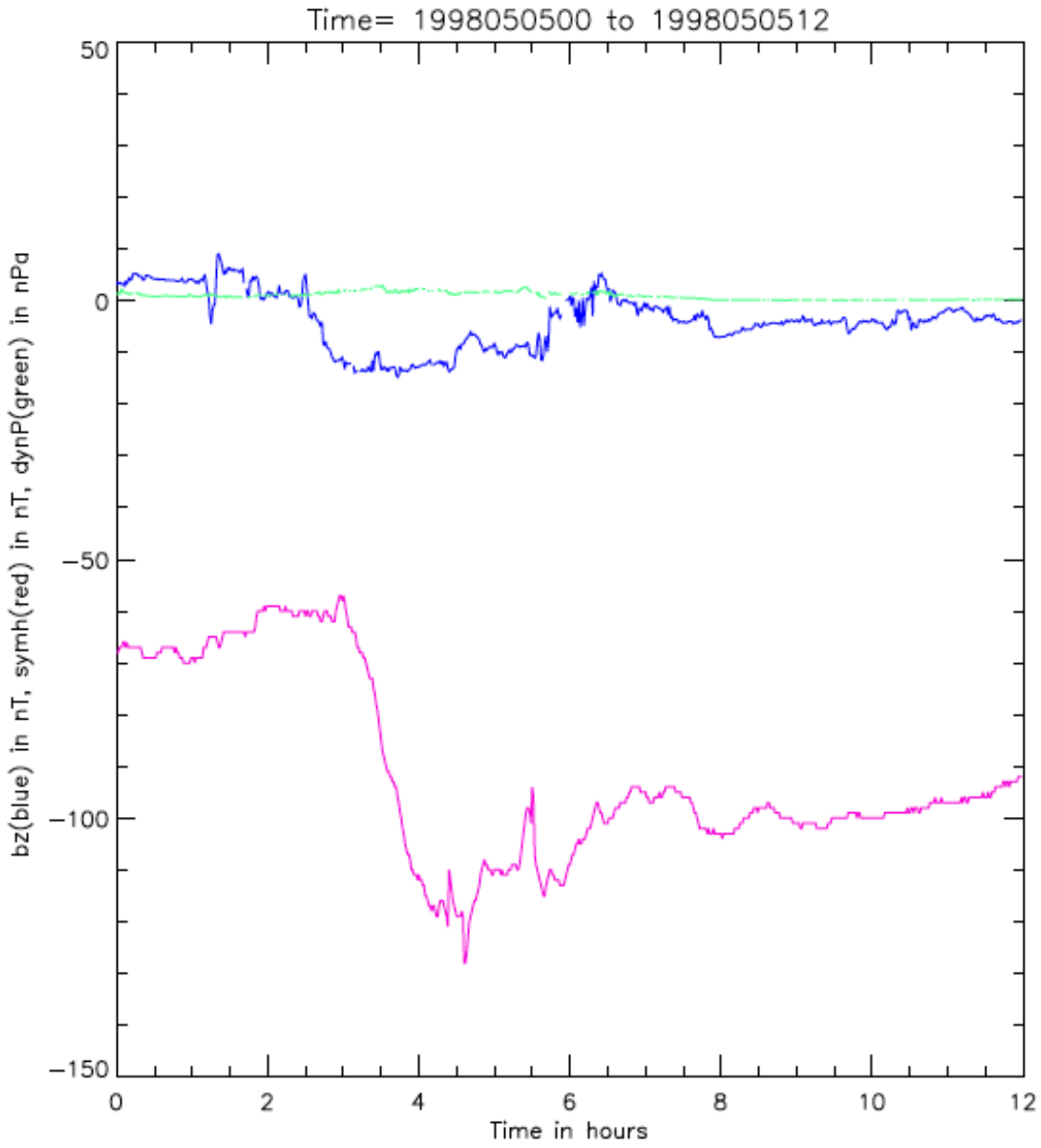

Figure 4.3: A graph for fluctuations of IMF B_Z (blue), sym-H (red) and the dynamic pressure of the solar wind (green) for May 5, 1998, starting at 00 UT and ends at 12 UT where Sym-H and IMF changed but the dynamic pressure of the solar wind is almost constant.

4.1.3 Case III: All the parameters (solar wind dynamic pressure and Sym-H) changing with time

An example of more normal case is illustrated in Figure 4.4, in which all the parameters (solar wind dynamic pressure and IMF) changed simultaneously. The time period of this case is from 00 UT on 4th May 1998 to 20 UT on 4th May 1998. Here, at the beginning, the dynamic pressure is around 0 nPa, the IMF B_Z is slightly negative and the Sym-H at the onset is around -50 nT. After a couple of hours the IMF B_Z undergoes a large negative excursion and the Sym-H follows suit going down to around -280 nT, which indicates a major magnetic storm. After a few hours, recovery begins but the Sym-H value is still much smaller than normal value. Clearly the strong negative drop in the Sym-H is triggered by a sudden turn to a negative IMF B_Z and there appears no effect associated with dynamic pressure.

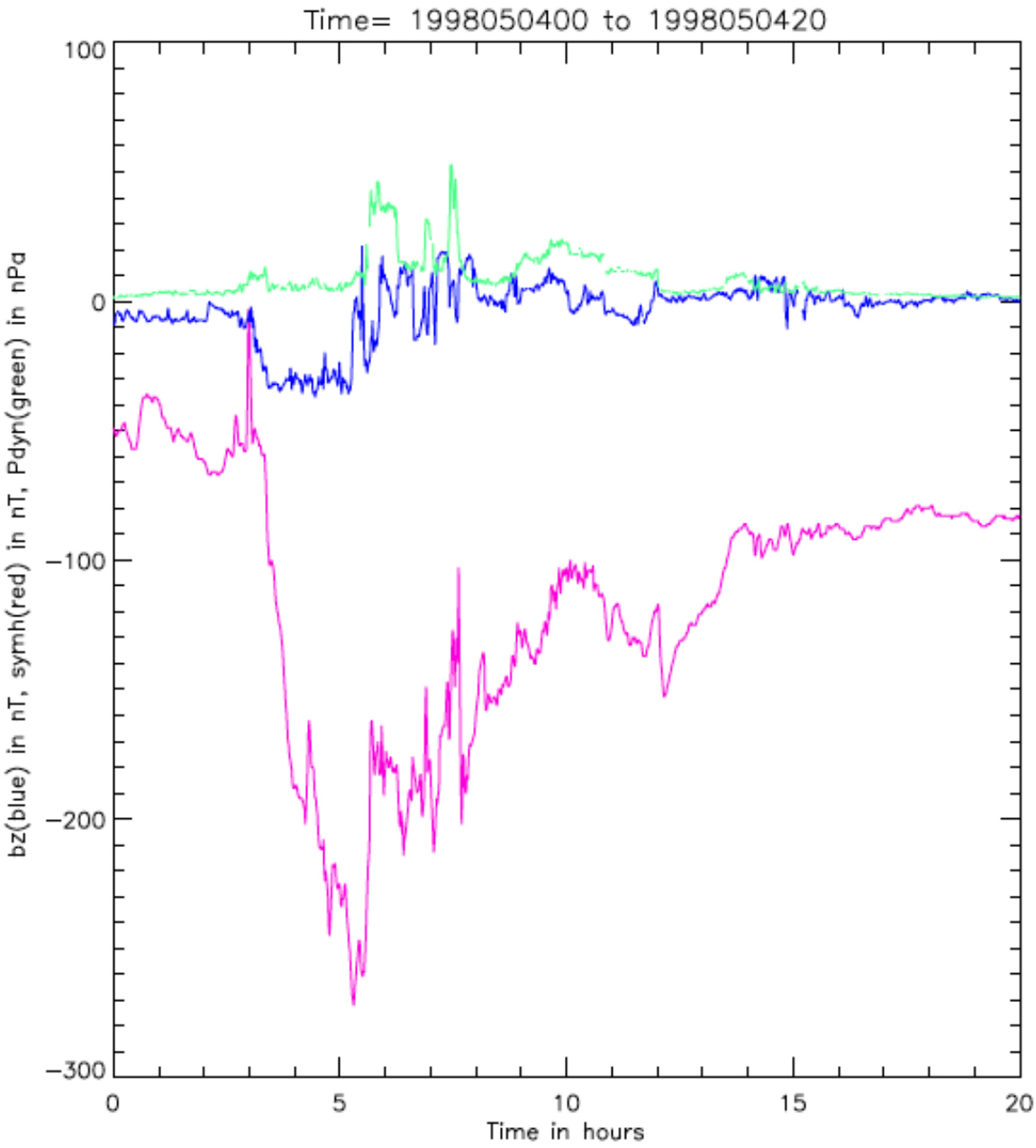

Figure 4.4: A graph for IMF Bz (blue), Sym-H (red) and the solar wind dynamic pressure (green) for May 4, 1998, starting at 00 UT and ends at 20 UT where the dynamic pressure and the IMF changed with time.

CHAPTER FIVE

DATA ANALYSIS

As alluded to in the previous chapter, it was not possible to carry out a statistical study of the effects of changing dynamic pressure alone due to a lack of sufficient events. This study looks at the events when one of the principal Sym-H controlling parameters (IMF B_Z and dynamic pressure of the solar wind) remains constant. *Gillies et. al., (2012)* characterized the ionospheric response to sudden commencement events where a sudden change in dynamic pressure is followed by sudden change in the Sym-H. Various authors before did almost the same thing. *Boudouridis e. al. (2007)* showed that an abrupt increase in solar wind dynamic pressure resulted in strong increase in the magnitude of the dayside convection velocities recorded by SuperDARN. This study looks at individual events to see if there is drastic change in the Sym-H following steep dynamic pressure changes. The three main data sets used in this thesis are Sym-H, the IMF and the dynamic pressure of the solar wind. Sym-H was choosen ahead of Dst because of its higher temporal resolution (one minute) (*Iyemori, 1990; Wanliss and Showalter, 2006*). The one-minute resolution of Sym-H agrees well with the two minutes resolution of SuperDARN data and one-minute resolution of the solar wind data. SuperDARN radars monitor plasma convection in the mid– to high- latitude ionosphere and provides convection maps for both the northern and southern hemispheres (*Greenwald et al., 1995; Ruohoniemi and Baker, 1998; Chisham et al., 2007*). So to analyze the data the northern hemisphere SuperDARN radars were used. *Gillies et al. (2012)* studied some sudden commencement events and characterized those using Sym-H data. The Sym-H returned to its pre-disturbed condition after the sudden

impulse (SI). In *Gillies et al. (2012)* sudden Impulse and storm sudden commencement events were both clearly related to sudden increase in the solar wind dynamic pressure. The Sym-H underwent decay10 minutes after the jump in the dynamic pressure even though the dynamic pressure of the solar wind remained high for a much longer time. The first focus of this thesis is to look at the events where sudden change in the dynamic pressure of the solar wind takes place and how the Sym-H responds to that change when there is no change in IMF B_Z and vice-versa. The events, discussed here, are divided into three categories, such as, (1) when the solar wind dynamic pressure changes but IMF B_Z remains constant, (2) when the dynamic pressure of the solar wind remains constant but IMF B_Z changes and (3) when both the IMF and the dynamic pressure change.

As described above, at first special attention was given to how Sym-H responds to dynamic pressure change in the absence of IMF B_Z changes and vice-versa. These kinds of phenomena are rare, particularly for isolated dynamic pressure variations. To find events of interest, we first looked randomly at the data. We chose the year 1998 and uncovered few events where it was easy to separate the two controlling parameters, solar wind dynamic pressure and interplanetary magnetic field. The three days when those events were occurring are 2nd May, 1998; 4th May, 1998 and 5th May, 1998. All the solar wind data came from the WIND satellite. The three different cases are discussed in the following sections.

5.1 Constant IMF B_Z with changing dynamic pressure:

First, this thesis deals with a case where the IMF B_Z remains constant for a certain period of time and Sym-H fluctuates along with the fluctuations of the dynamic pressure of the solar wind. The time period for this first case covers from 18 UT on 2nd May 1998 to 20 UT on 3rd May 1998. In

this time period the IMF B_Z remains almost constant for several hours while the dynamic pressure changes a lot and the Sym-H responds in clear fashion. This interval of interest is shown in Figure 5.1.

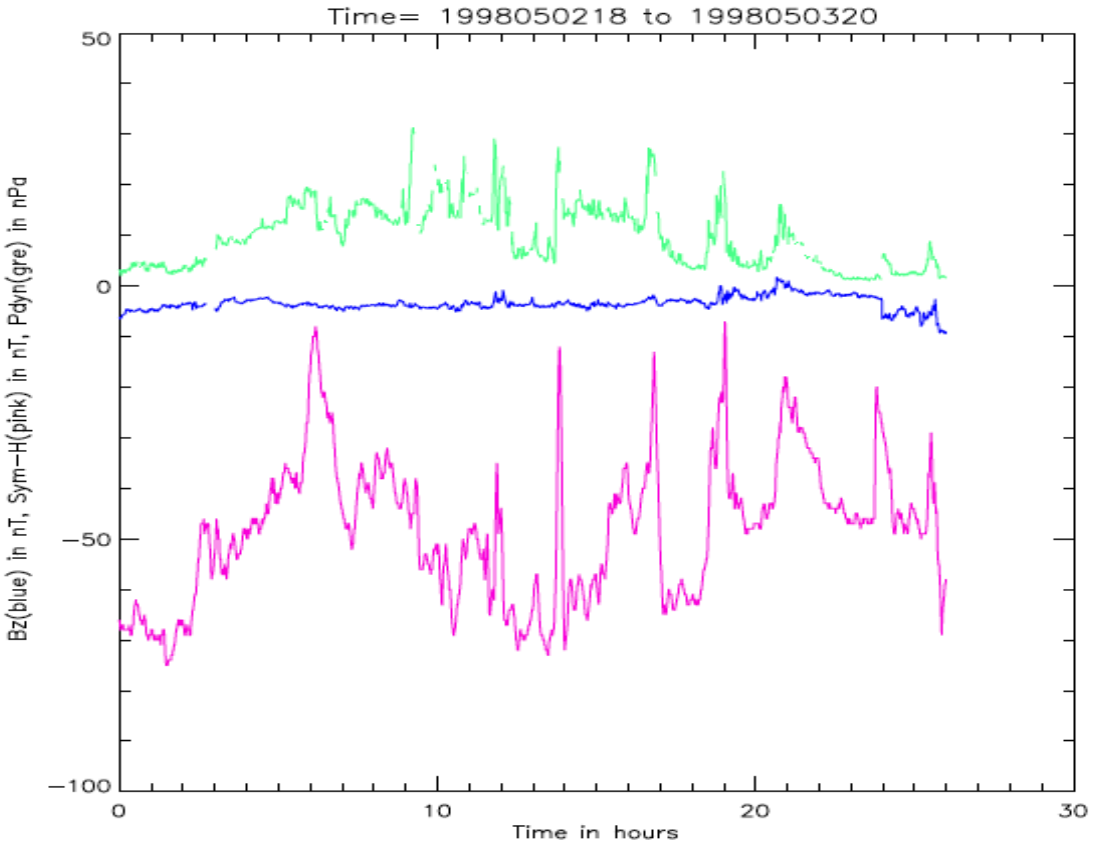

Figure 5.1: Fluctuations of Sym-H (pink line) with the dynamic pressure of the solar wind (green line) for a period of minimal changes in the IMF B_Z (blue line) for the time period from 18 UT on 2nd May 1998 to 20 UT on 3rd May 1998.

To put the event of interest in context we display data starting at few hours ahead of the event (Figure 5.2). In Figure 5.2 time starts from from 00 UT on 2nd May 1998 to 19 UT on 3rd May 1998. Here we see that Sym-H drops to a large negative value at first due to a large negative

change in IMF B_Z. The result was a medium strength magnetic storm with B_Z remaining constant during a recovery phase for a long time. From Figure 5.2 we see a large change in Sym-H at the beginning of the time period, going to a maximum negative value of -75 nT. At the same time B_Z also goes down and reaches its minimum value one hour before Sym-H reaches its maximum negative value, in agreement with previous findings by *Gillies et al* (2012) and references therein. This definitely shows that the event under study is a magnetic storm. Also worthy of notice is that at the beginning of the time period B_Z reaches -10 nT and stays negative for a couple of hours. The IMF B_X also starts with a very large negative value. For the next couple of hours, B_X retains a large negative value before jumping to a large positive value nine hours after the starting time.

The IMF B_Y also had rather large values in the range of -10 nT to +10 nT throughout the time period. The dynamic pressure also undergoes considerable fluctuations, especially in the recovery phase of the storm, at the same time when B_Z stays almost constant. At the recovery phase IMF B_Z started to reach normal values and reach around 5 nT value and maintain this value for a long time. The IMF B_Z remains constant for the time period of from 18 UT on 2nd May 1998 to 20 UT on 3rd May 1998. In this time period Sym-H fluctuated along with the solar wind dynamic pressure.

From Figure 5.3 we see at 19 UT on day May 2 of 1998, Sym-H has a high negative value of around 60 nT. In the time period from 18 UT on 2nd May 1998 to 20 UT on 3rd May 1998 Sym-H fluctuated from -20 nT to -60 nT. There are lots of Sym-H peaks. The peaks are closely related to dynamic pressure peaks but the magnitude of the response changes a lot. Then the question is what is responsible for the amplitude in the Sym-H response?

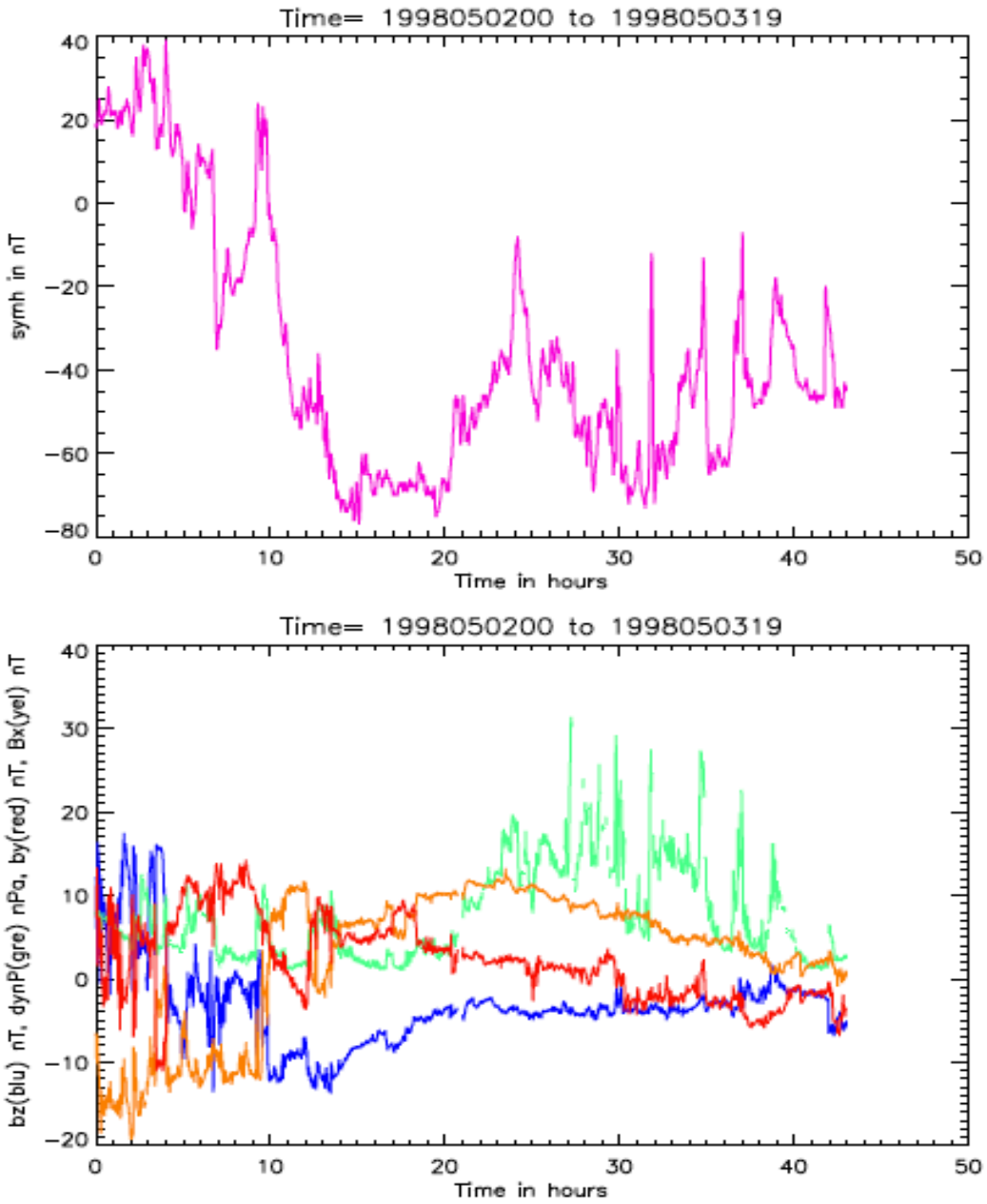

Figure 5.2: comparison of the IMF parameters with the Sym-H (pink) and the dynamic pressure (green) for the time period from 00 UT on 2nd May 1998 to 19 UT on 3rd May 1998. The top row is for Sym-H and the bottom row is for the IMF parameters and the dynamic pressure. Green line: dynamic pressure, Blue line: IMF Bz, Red line: IMF By, Yellow line: IMF Bx.

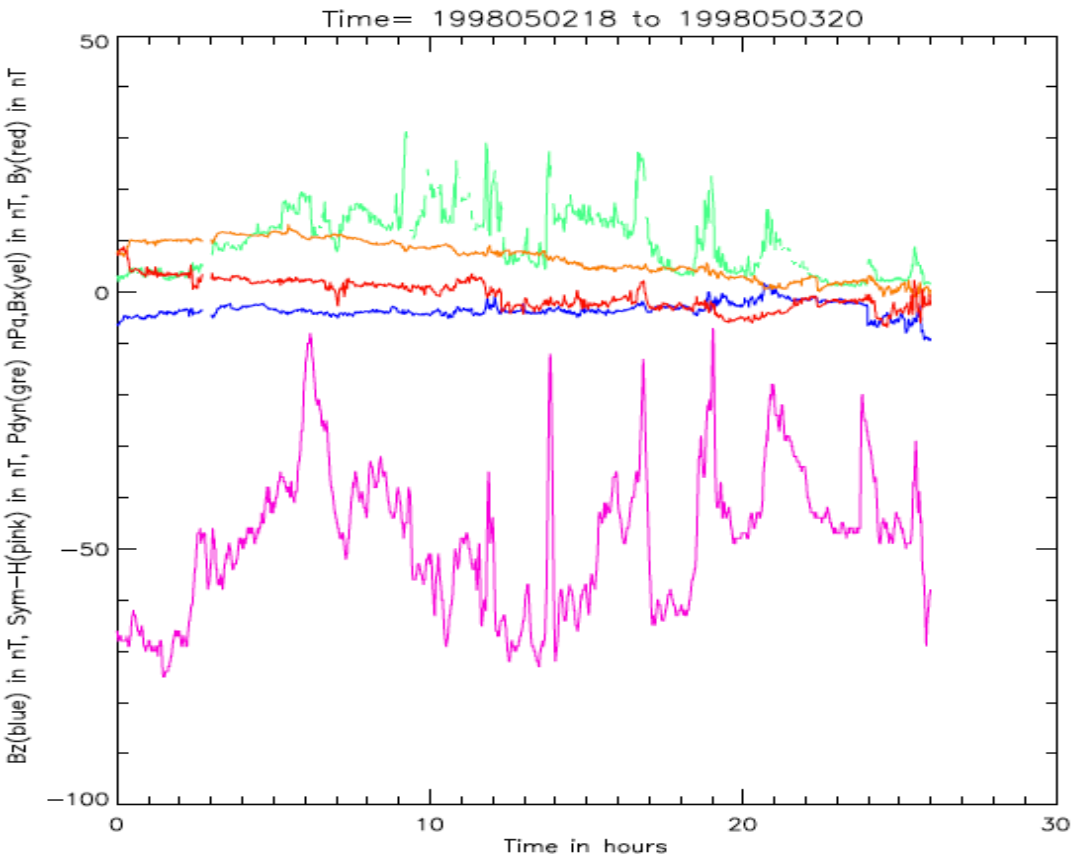

Figure 5.3: A graph for IMF B_X (yellow), IMF B_Y(red), and IMF B_Z(blue) data, Sym-H (pink) and dynamic pressure (green) where time starts at 18 UT on May 2 of 1998 and ends at 20 UT on May 3, 1998.

To find the answer, various scatter plots of Sym-H versus dynamic pressure of solar wind were plotted. Figure 5.4 shows a scatter plot of Sym-H versus the solar wind dynamic pressure for different classes of the magnitude of B_Y. In this graph, dynamic pressure is on the x-axis and Sym-H on the y-axis. It shows that the response of Sym-H to the dynamic pressure of the solar wind is not influenced by the magnitude of IMF B_Y as we see the points are all over the plot without any connection to the B_Y magnitude. We made a similar plot for B_X. As seen in Figure

5.5, we find that for different values of B_X we have different Sym-H responses to the solar wind dynamic pressure. However, when B_X is less than 5 nT the effect of dynamic pressure on Sym-H is not clear. For <5 nT the points spread all over the graph just like they did for the magnitude of B_Y. But, as we go to higher values of B_X we see a strong relation between dynamic pressure and Sym-H. The larger values of B_X produce a stronger relation between dynamic pressure and Sym-H. We have red points for 5-9 nT of B_X and blue points for >9 nT. This suggests that when B_X exceeds the magnitude of B_Z, which is 5 nT in the present case, there is a stronger connection between the dynamic pressure of the solar wind and the Sym-H.

5.2 Constant dynamic pressure and changing IMF Bz:

The next case study is for when the dynamic pressure of the solar wind remains constant while the IMF B_Z changes. The time period for this graph is from 00 UT on 5th May 1998 to 12 UT on 5th May 1998. If we look at Figure 5.6 we see IMF B_Z starts with a positive value and Sym-H with a large negative value. After two and a half hours the IMF B_Z goes negative by 20 nT. After a few minutes of transition in the IMF B_Z, Sym-H undergoes a steep decrease and maintains negative large value for the rest of the time period. Clearly, here Sym-H follows B_Z, much as had been found in the past (e.g. *Gillies et al., 2011*). However, previous studies have shown that there was a 1 to 2 hours delay between the time when the IMF B_Z reaches at its minimum and the time at which a storm would enter its recovery phase (e.g. *Gillies et al., 2011*, and references therein).

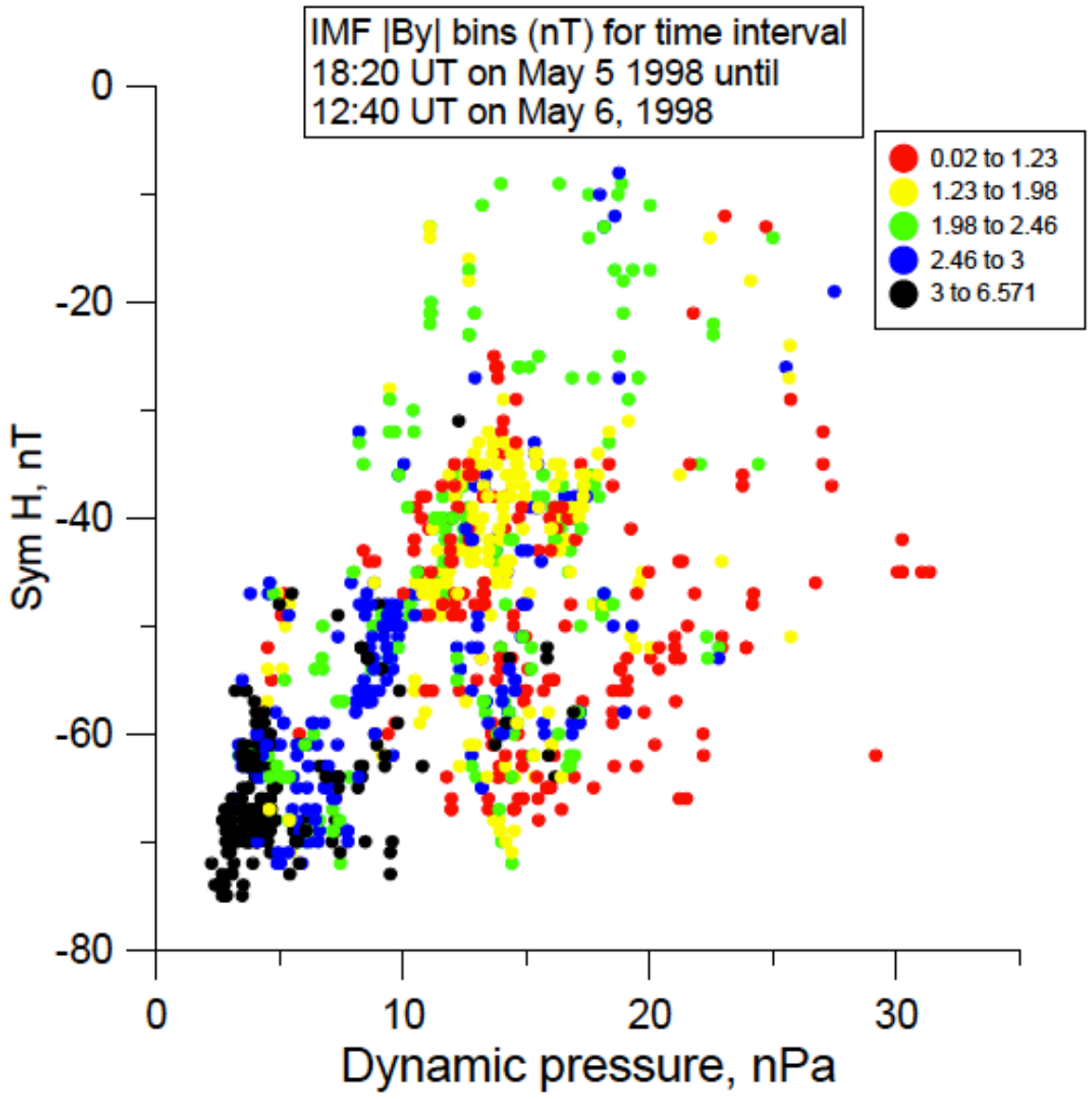

Figure 5.4: Scatter plot of Sym-H versus dynamic pressure for the different classes associated with the magnitude of B_y in nT. Red dots are for 0.02 to 1.23 nT, yellow dots are for 1.23 to 1.98 nT, green dots are for 1.98 to 2.46 nT, blue dots are for 2.46 to 3 nT, and black dots are for 3 to 6.571 nT.

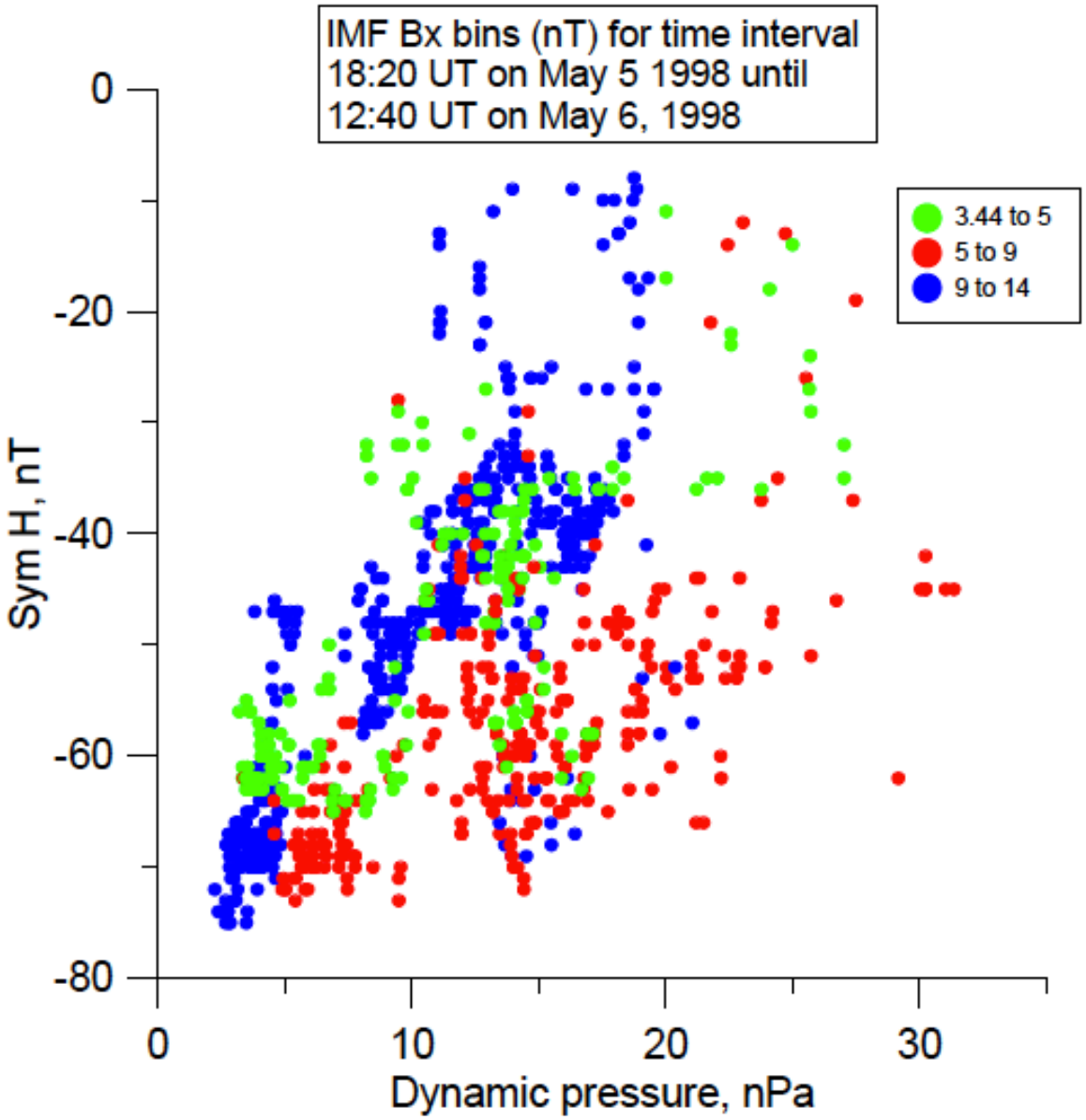

Figure 5.5: Scatter plot of Sym-H versus dynamic pressure for different classes of B_x values in nT. Green dots are for 3.44 to 5 nT, red dots are for 5 to 9 nT, and blue dots are for 9 to 14 nT.

To see what kinds of time delays would be associated with the present example, few scatter plots of B_Z vs Sym-H for different time lags were produced. We chose 15, 30, 45, 60, 75 and 90 minutes lag for Sym-H. The results are shown in Figures 5.7 (a), Figures 5.7 (b), Figures 5.7 (c), Figures 5.7 (d), Figures 5.7 (e), Figures 5.7 (f). From these plots we could clearly see that for less than 60 minutes delay times, there would be horizontal arrangements of dots at large negative B_z values on the plots. As we go for time lag more than 60 minutes the horizontal points vanishes and a reasonable correlation can be seen between the IMF B_Z and the Sym-H values. This shows that in between 60 to 90 minutes time lag the maximum negative value of Sym-H coincides with the maximum negative value of IMF B_Z, in accordance with previous work. The only difference here with previous work done by *Gillies et al.,* (2011) is that we could establish the link of the time delay in the absence of any dynamic pressure fluctuations.

5.3 A more normal situation: simultaneous changes in the dynamic pressure and the IMF B_Z:

In a third case shown in Figure 5.8, both the IMF B_Z and the dynamic pressure of the solar wind undergo simultaneous changes. The time period of this graph is from 00 UT on 4th May 1998 to 20 UT on 4th May 1998. Here at the beginning the dynamic pressure is around 0 nPa, while the IMF B_Z is slightly negative and Sym-H is around -50 nT. Two hours later the IMF B_Z goes to a large negative value and the Sym-H undergoes a large negative fall down to around -280 nT. After few hours there has been a strong recovery phase even though the Sym-H value is still as

low as -100 nT. If we look at the solar wind parameters we see that Sym-H was triggered by a sudden change in the IMF B_Z but there was not too much effect of the large change of dynamic pressure of the solar wind on the Sym-H. After first five hours when the IMF B_Z goes closer to 0 nPa, the Sym-H becomes less negative. However there are now oscillations in the Sym-H that are clearly associated with dynamical pressure variations. This behavior is in agreement with our earlier findings regarding the effects of the solar wind dynamic pressure change on the Sym-H.

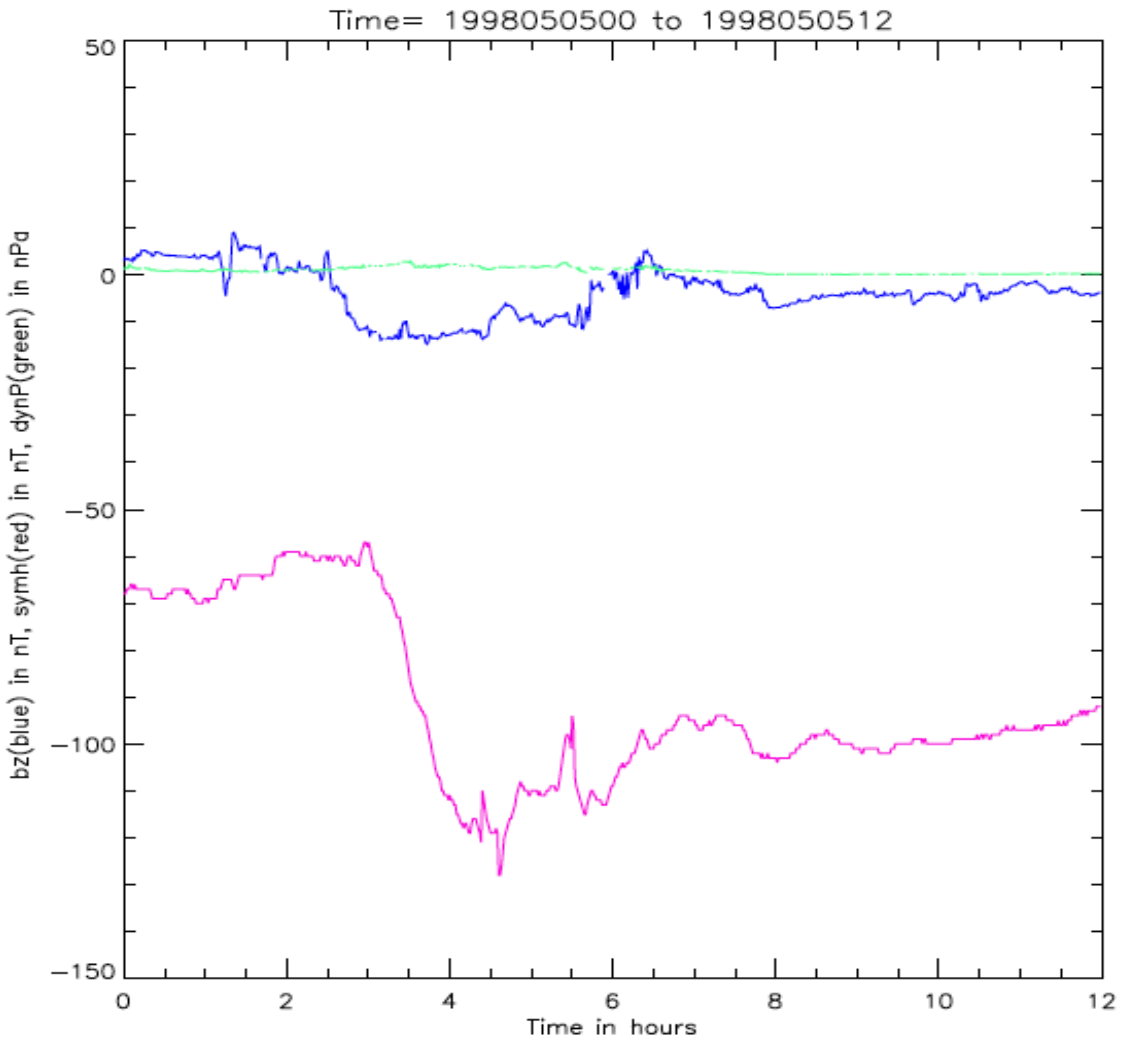

Figure 5.6: A graph for IMF Bz (blue), Sym-H (red) and dynamic pressure (green) of the solar wind for the time period from 00 UT on May 5, 1998 to 12 UT on May 5, 1998, where the solar wind dynamic pressure is almost constant while the IMF Bz goes to a large negative value.

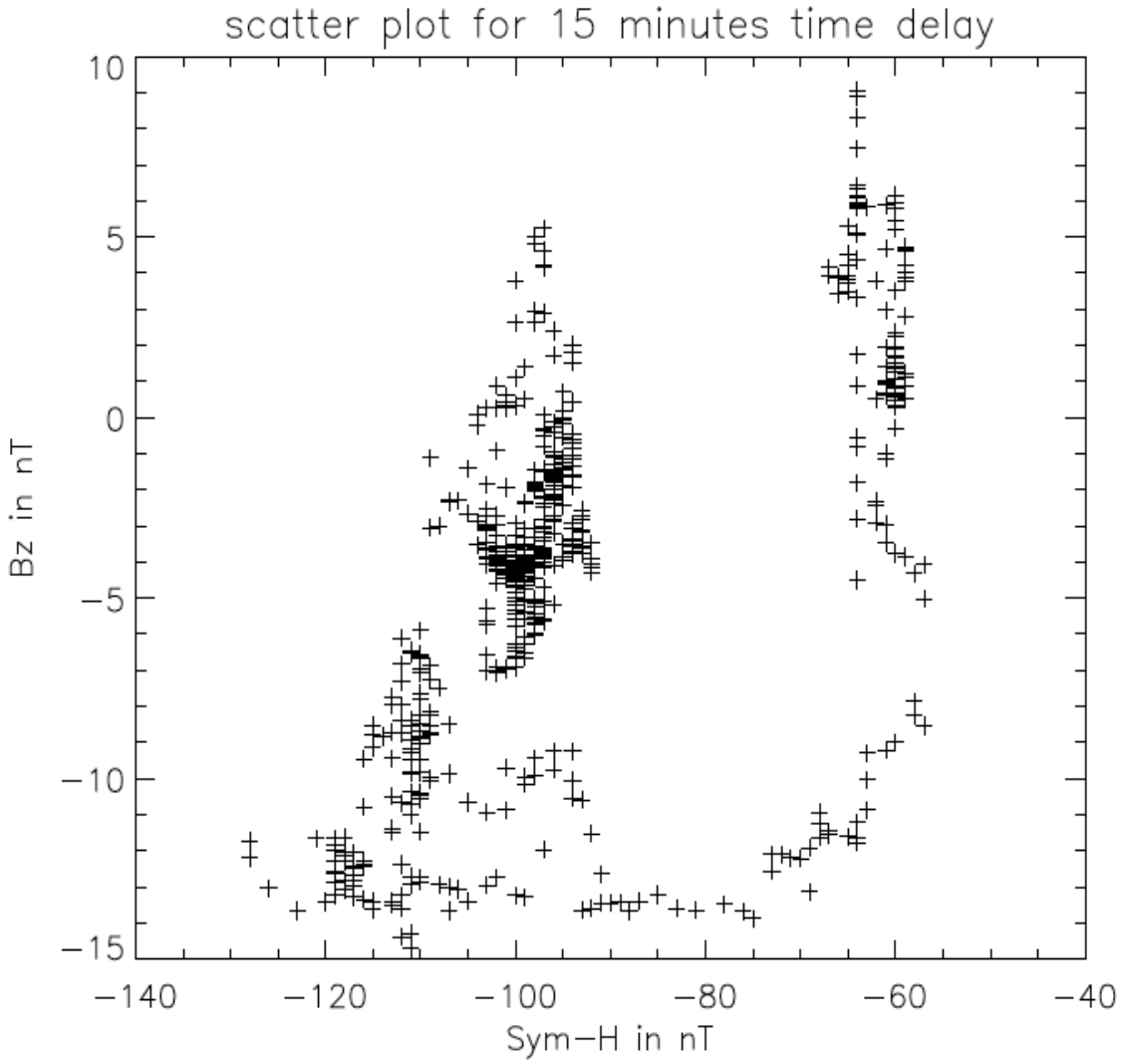

Figure 5.7: (a) Scatter plots of B_Z and Sym-H for 15 minutes time lags where B_Z at the vertical and Sym-H at horizontal.

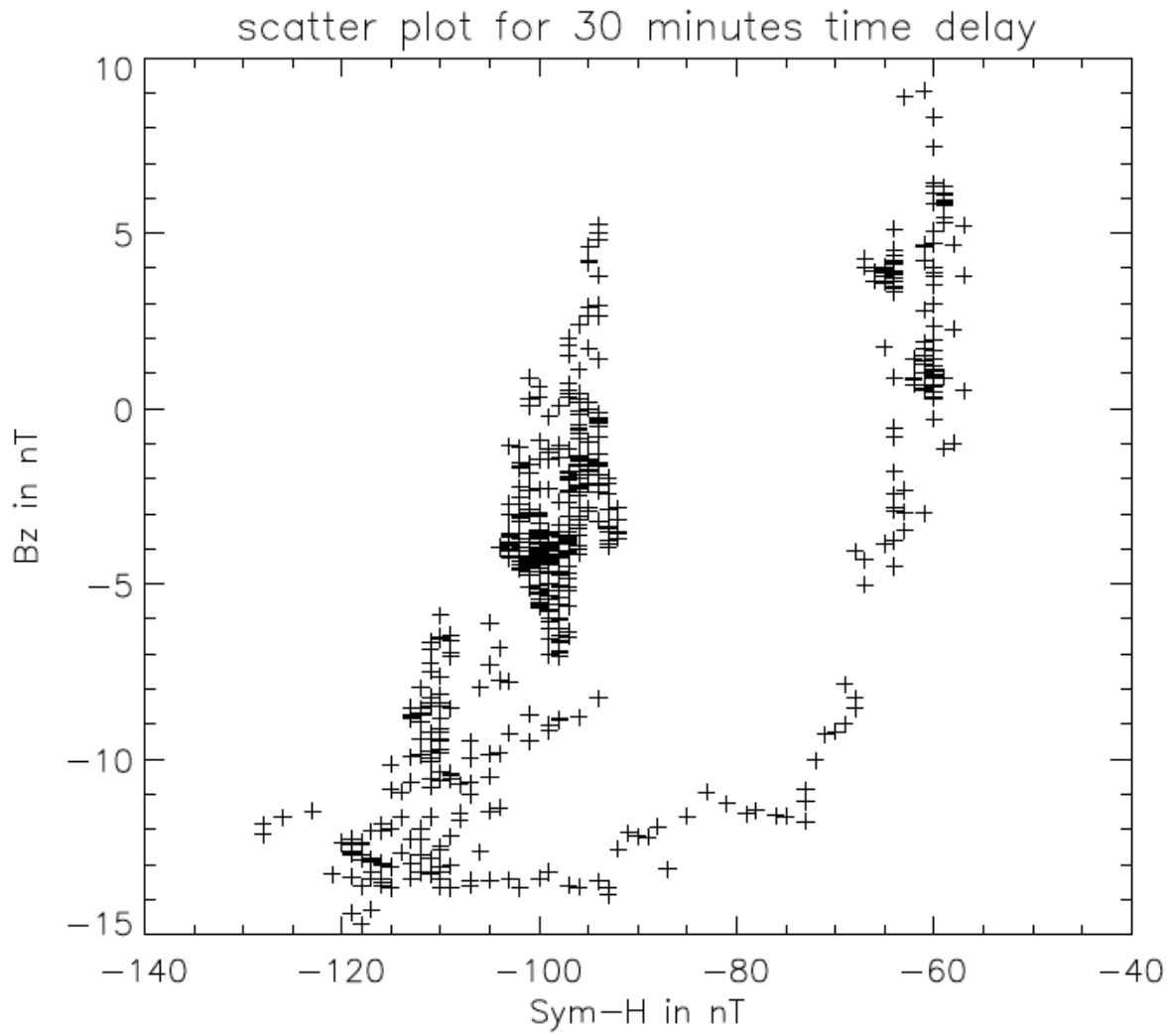

Figure 5.7: (b) Scatter plots of B_Z and Sym-H for 30 minutes time lags where B_Z at the vertical and Sym-H at horizontal.

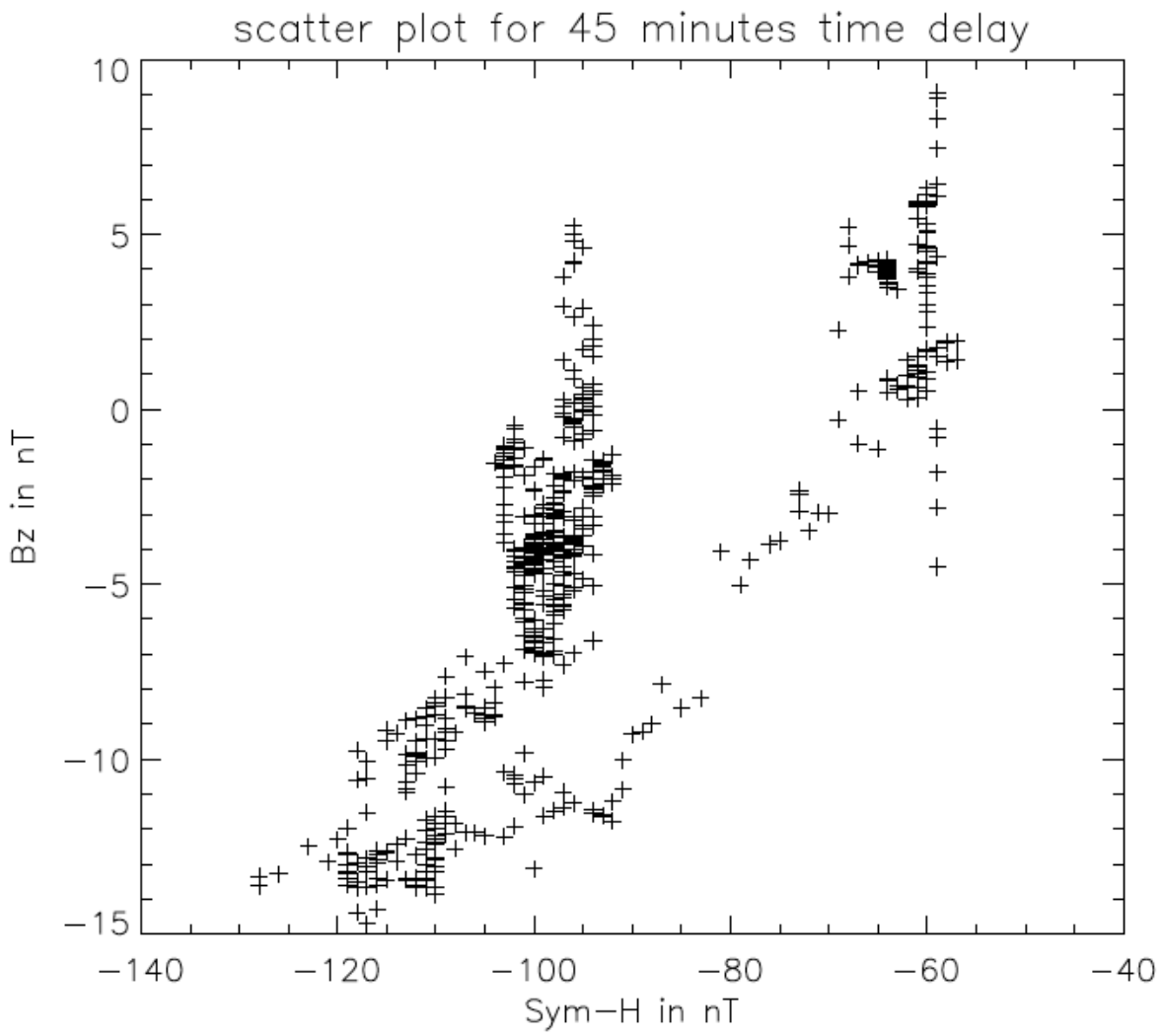

Figure 5.7: (c) Scatter plots of B_z and Sym-H for 45 minutes time lags where B_z at the vertical and Sym-H at horizontal.

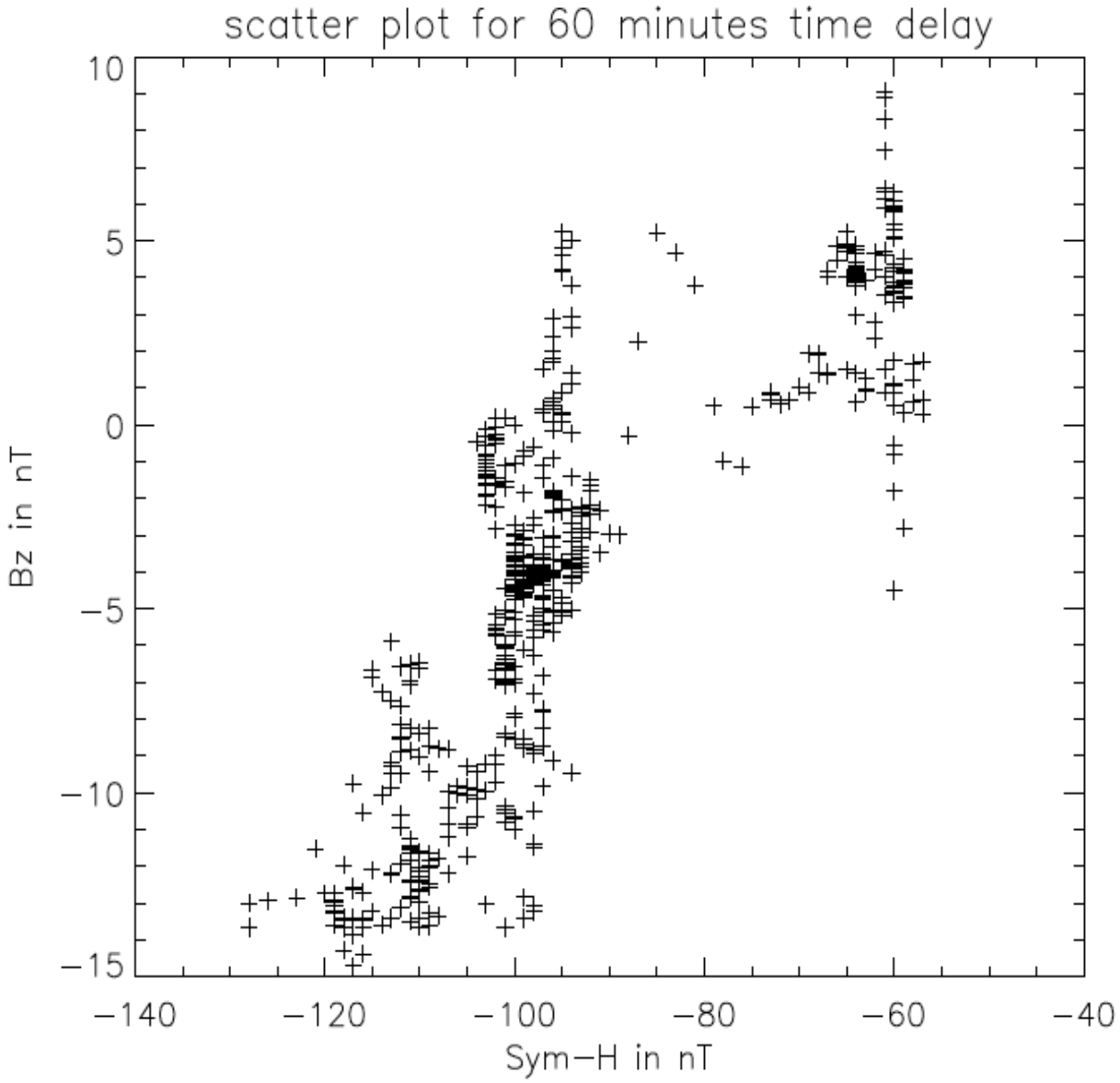

Figure 5.7: (d) Scatter plots of B_Z and Sym-H for 60 minutes time lags where B_Z at the vertical and Sym-H at horizontal.

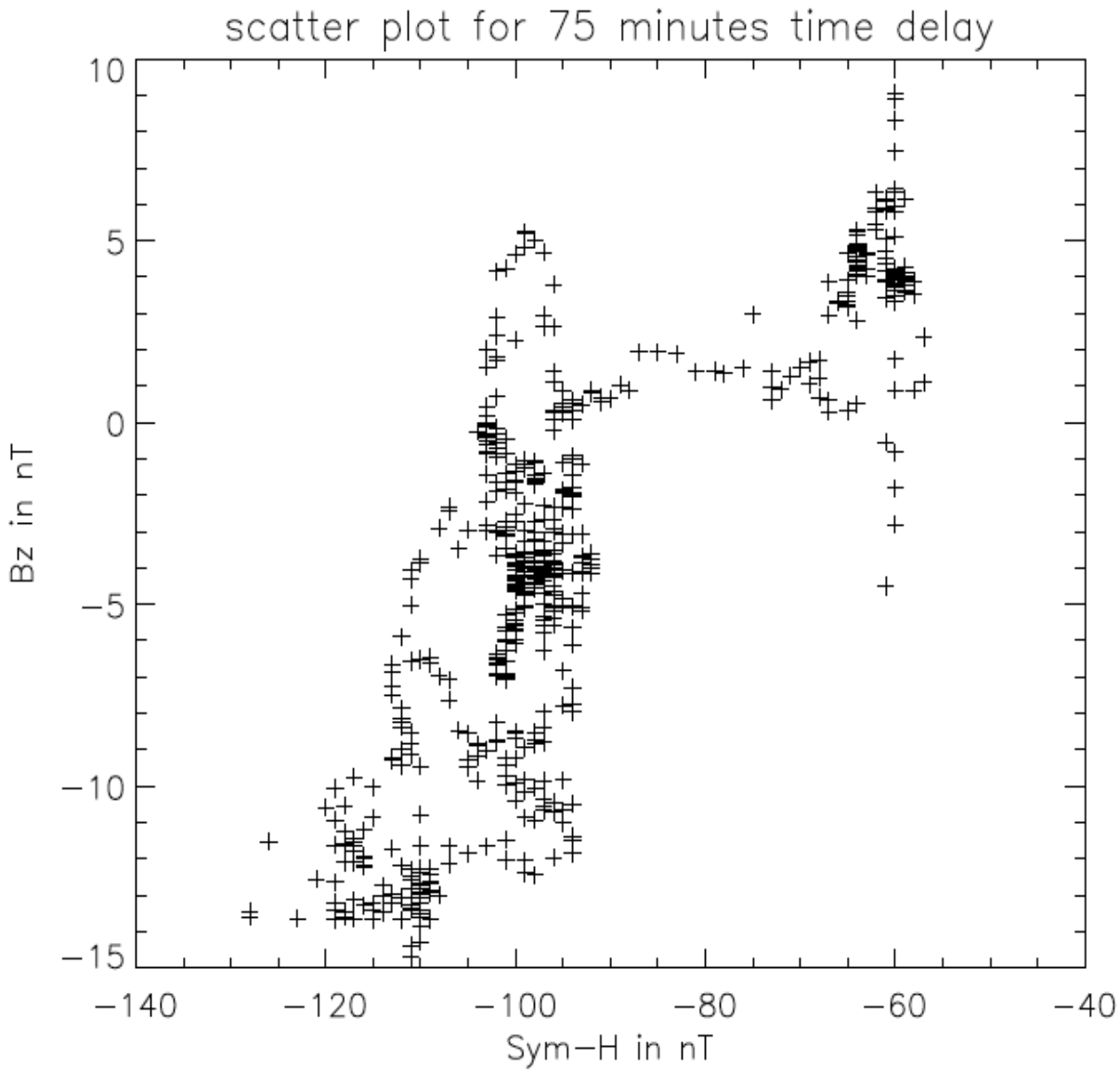

Figure 5.7: (e) Scatter plots of B_Z and Sym-H for 75 minutes time lags where B_Z at the vertical and Sym-H at horizontal.

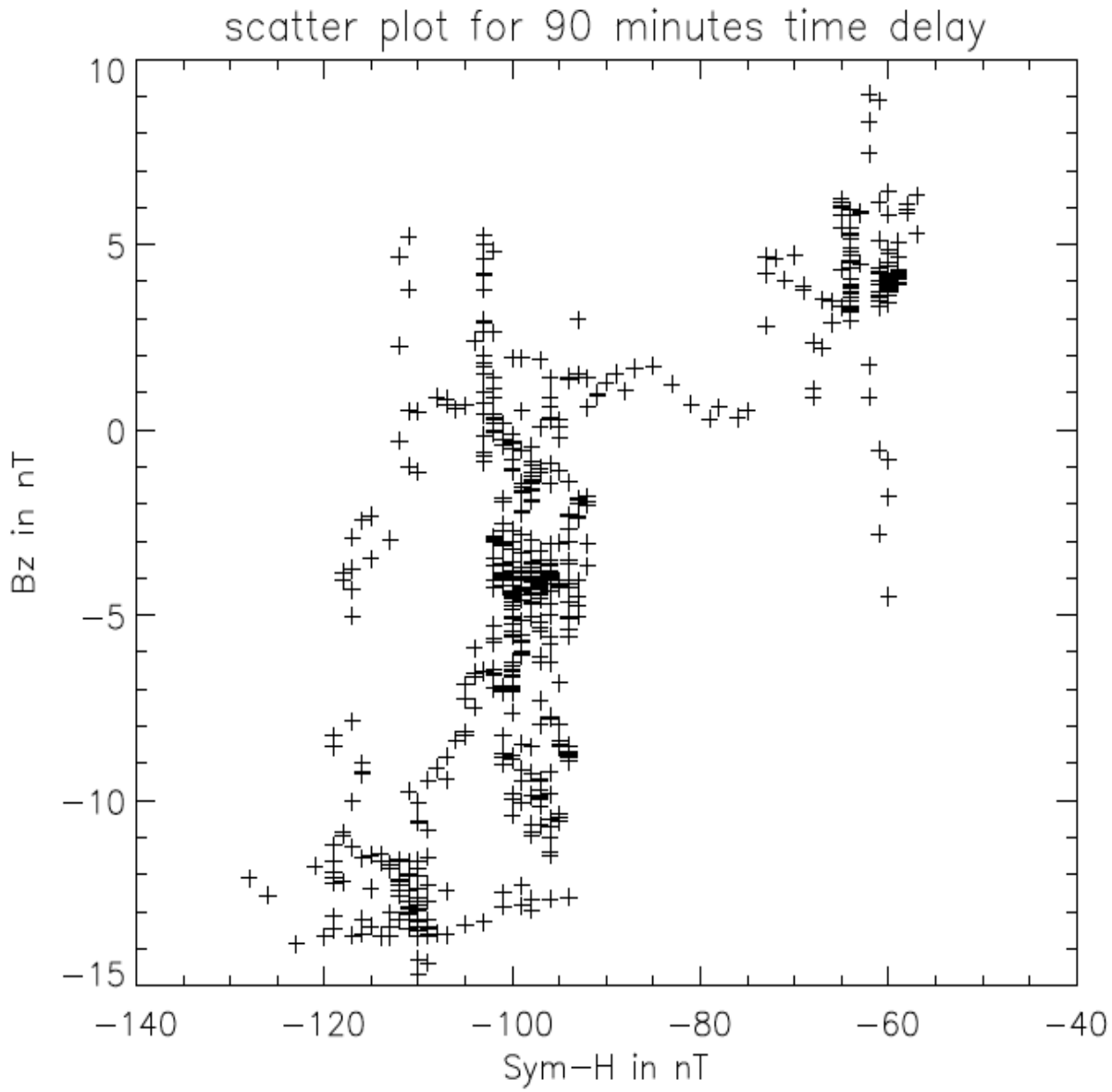

Figure 5.7: (f) Scatter plots of B_z and Sym-H for 90 minutes time lags where B_z at the vertical and Sym-H at horizontal.

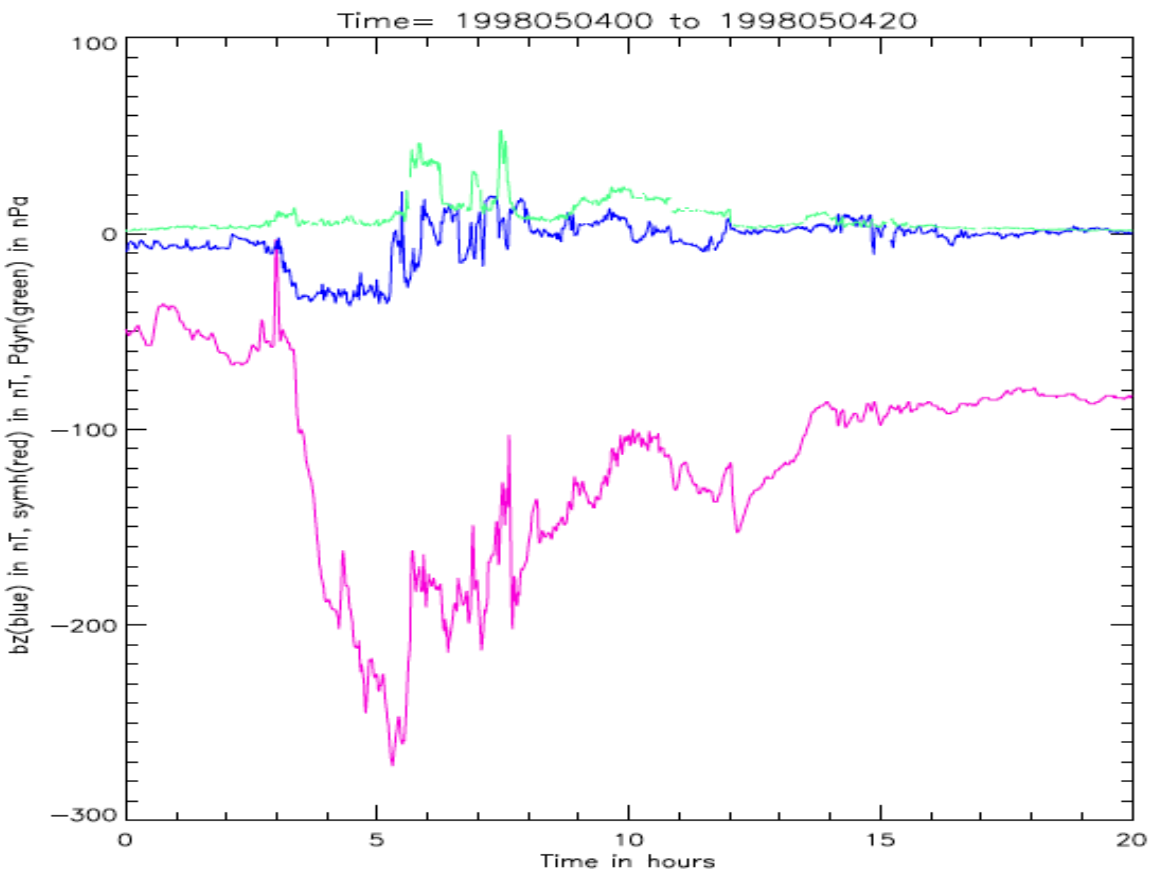

Figure 5.8: A graph for IMF Bz (blue), Sym-H (red) and the solar wind dynamic pressure (green) for May 4, 1998, starting at 00 UT and ends at 20 UT where the dynamic pressure and the IMF changed with time.

CHAPTER SIX

CONCLUSION AND FUTURE WORK

This study investigated the separate roles played by the solar wind dynamic pressure and the north-south component of the interplanetary magnetic field (IMF B_z) on the Sym-H index. The dynamic pressure and the IMF B_z are usually both changing during a magnetic storm. This is related in part to the fact that when the solar wind is compressed (increased density or velocity), the magnitude of the IMF is amplified. Nevertheless, the IMF B_z and the solar wind dynamic pressure impact the Sym-H index through very different mechanisms. The impact of dynamic pressure is felt because compression of the magnetosphere caused by plasma pressure carried by the solar wind forces the magnetopause to move closer to earth and as a response to this compression the geomagnetic field increases. This is due to an increase in the magnetopause current past the bow shock. By contrast the IMF B_z (that is, the component of the north-south interplanetary magnetic field) affects the Sym-H by causing an increase in the ring currents that circle the earth. This is the end result of a cascade of events that starts with an increase in the reconnection rate up front (in the noon sector), which creates a pile-up of plasma in the geomagnetic tail. When the IMF B_z turns northward at the end of an event, the magnetotail empties itself by injecting particles in the ring currents, which, over time, weaken as they lose charged particles (a storm recovery phase).

This thesis uncovered some rare events for which there was no simultaneous change in the IMF B_Z and the solar wind dynamic pressure. This helped address the question: if the dynamic pressure suddenly weakens, does the Sym-H index suddenly go down? And if so, how

predictable is the decrease in the Sym-H for a given decrease in the dynamic pressure? We could also address the question of how much the Sym-H is affected purely by changes in the IMF B_z in rare cases for which there is no accompanying change in the solar wind dynamic pressure.

The present study has shown that changes in the dynamic pressure can create undulations in the Sym-H that have nothing to do with IMF B_z changes and/or with magnetic substorms. It was found in one particularly clear event that when the dynamic pressure goes down, there is an accompanying decrease in the Sym-H. However, the decrease was not predictable just in terms of the change in the dynamic pressure. Something else affected the magnitude of the Sym-H response. In the event under consideration, for a given IMF B_z, the response was not affected by the IMF B_y but appeared to be strongly controlled by the IMF B_x as long as the latter had a greater magnitude than that of the IMF B_z. As soon as the IMF B_x value went larger than Bz there started to be a strong relation between Sym-H and dynamic pressure.

In a second special case the dynamic pressure of the solar wind was constant while changes in the IMF B_z were behind important Sym-H changes. This kind of situation is not a regular occurrence either. Scatter plots for this second type of event were used to uncover the relation between Sym-H and the B_z component of the interplanetary magnetic field. From the scatter plots there is clear evidence for a 60 to 90 min delay between the time when the Sym-H reaches its maximum negative value and the time when the Bz goes through its minimum. This time scale is comparable to that which has been uncovered in the past (*Gillies et al, 2012* and references therein).

It would be of interest to uncover more events of the kinds that were found in the present work. The general conditions for the observation considered here were multiple CME's (Coronal mass

ejections). Also, occurrences of steady or slowly changing IMF are usually associated with "magnetic clouds". Further studies will be required to more specifically find the reason behind the kind of behaviour found in the solar wind parameters, allowing researchers to hopefully include more events so as to be able to draw more definitive conclusions.

As just eluded to, it was not possible to perform a statistical analysis of our findings, due to lack of sufficient events. The lack of statistics also meant that little information could be extracted from the SuperDARN radars, which at first were going to be part of this study. The primary research goal in this work was to find some events where the solar wind dynamic pressure underwent multiple drastic changes in the absence of IMF modulations and vice-versa. This was to be followed by an analysis of the effects on the convection pattern based on SuperDARN data. Unfortunately, a large enough number of events were not found to date. There is still hope in the future to uncover a wide enough range of events to enable a statistical study of the response of convection based on SuperDARN data.

REFERENCES

Akasofu, S.-I., and S. Chapman (1963b), Magnetic storms: The simultaneous development of the main phase (DR) and of polar magnetic substorms (DP), J. Geophys. Res., 68 (10), 3155–3158, doi:10.1029/JZ068i010p03155

Alves, M. V., E. Echer, and W. D. Gonzalez (2006), Geoeffectiveness of corotating interaction regions as measured by Dst index, J. Geophys. Res., 111 (A07S05), doi:10.1029/2005JA011379.

Baker, K. B., and S. Wing (1989), A new magnetic coordinate system for conjugate studies at high latitudes, J. Geophys. Res., 94 (A7), 9139–9143, doi: 10.1029/JA094iA07p09139.

Borovsky, J. E., and M. H. Denton (2010), Solar wind turbulence and shear: A superposedepoch analysis of corotating interaction regions at 1 AU, J. Geophys. Res., 115 (A10101), doi:10.1029/2009JA014966.

Boudouridis, A., L. R. Lyons, E. Zesta, and J. M. Ruohoniemi (2007), Dayside reconnection enhancement resulting from a solar wind dynamic pressure increase, J. Geophys. Res., 112 (A06201), doi:10.1029/2006JA012141.

Brueckner, G., and J.-D. F. Bartoe (1983), Observations of high-energyjets in the corona above the quiet sun, the heating of the corona, and the acceleration of the solar wind, The Astrophysical Journal, 272, 329–248.

Chisham, G., et al., (2007), A decade of the Super Dual Auroral Radar Network (SuperDARN): scientific achievements, new techniques and future directions, Surv. Geophys., 28, 33–109, doi:10.1007/s10712–007–9017–8.

Cliver, E. W., and A. G. Ling (2001),Coronal Mass Ejections Open Magnetic Flux and Cosmic-Ray Modulation, The Astrophysical Journal, 556 (1), 432, doi: 10.1086/321570.

Coco, I., E. Amata, M.F. Marcucci, M. De Laurentis, J.-P. Villain, C. Hanuise, and M. Candidi (2005), Effects on SuperDARN HF radar echoes of sudden impulses of solar wind dynamic pressure, Ann. Geophys., 23 (5), 1771–1783, 2005.

Gillies, D., K.A. McWilliams, J.-P. St.-Maurice, and S. Milan (2011), Global-scale observations of ionospheric convection during geomagnetic storms, J. Geophys. Res., 116 (A12238), doi:10.1029/2011JA017086.

Gillies, D. M., J.-P. St.-Maurice, K. A. McWilliams, and S. Milan (2012), Globalscale observations of ionospheric convection variation in response to sudden increases in the solar wind dynamic pressure, J. Geophys. Res., 117 (A04209), doi: 10.1029/2011JA017255.Heber, B., T.R Sanderson, and M. Zhang (1999), Corotating interaction regions, Advances in Space Research, 23 (3),567–579, doi:10.1016/S0273–1177(99)80013–1.

Gonzalez, W.D., Joselyn, J.A., Kamide, Y., Kroehl, H.W., Rostoker, G., Tsurutani, B.T., Vasyliunas, V.M., 1994, "What is a geomagnetic storm?", J. Geophys. Res. , 99 , 5771

Greenwald, R. A., W. A. Bristow, G. J. Sofko, C. Senior, J.-C. Cerisier, and A. Szabo (1995), Super Dual Auroral Radar Network radar imaging of dayside high-latitude convection under northward interplanetary magnetic field: Toward resolving the distorted two-cell versus multicell controversy, J. Geophys. Res., 100 (A10), 19661– 19674, doi:10.1029/95JA01215.

Illing, R. M. E., and A. J. Hundhausen (1983), Possible observation of a disconnected structure in a coronal transient, Geophysical Research Letters, 88 (A12), 10,210–10,214.

Perrault, P., and S.-I. Akasofu (1978), A study of geomagnetic storms, Geophys. J. R. Astr. Soc., 54, 547–573, doi:10.1111/j.1365-246X.1978.tb05494.x

Priest, E.R. (1997), edited by: Margaret G. Kivelson and Christopher T. Russell, Introduction to Space Physics, Cambridge University Press, Third Edition, 58–90.

Richardson, I. G., (2004). Energetic particles and corotating interaction regions in the solar wind, Space. Sci., 111, 267-376.

Ruohoniemi, J. M., and K. B. Baker (1998), Large-scale imaging of the high-latitude convection with Super Dual Auroral Radar Network HF radar observations, J. Geophys. Res., 103 (A9), 20797–20811, doi:10.1029/98JA01288.

Shue, J.-H., Chao, J.K., Fu, H.C., Russell, C.T., Song, P., Khurana, K.K., Singer, H.J., 1997, "A new functional form to study the solar wind control of the magnetopause size and shape", J. Geophys. Res. , 102 , 9497

Southwood, D.J., Kivelson, M.G., 2001, "A new perspective concerning the influence of the solar wind on the Jovian magnetosphere", J. Geophys. Res. , 106 , 6123–6130

Temmer, M., A. M. Veronig, E. P. Kontar, S. Krucker and B. Vrˇsnak (2010), Combined STEREO/RHESSI Study of Coronal Mass Ejection Acceleration and Particle Acceleration in Solar Flares, The Astrophysical Journal, 712, 1410, doi: 10.1086/0004-637X/712/2/1410.

Tokman, M., and P. Bellan (2002), Three-dimensional model of the structure and evolution of coronal mass ejections, The Astrophysical Journal, 567, 2002.

Vasyliunas, V.M., 1975, “Theoretical models of magnetic field line merging. I”, Rev. Geophys. Space Phys. , 13 , 303–336

Wanliss, J. A., and K. M. Showalter (2006), High-resolution global storm index: Dst versus Sym-H, J. Geophys. Res., 111 (A02202), doi:10.1029/2005JA011034.

Webb, D. F., and R. A. Howard (1994), The Solar Cycle Variation of Coronal Mass Ejections and the Solar Wind Mass Flux, J. Geophys. Res., 99 (A3), 42014220, doi:10.1029/93JA02742

Weimer, D. R., D. M. Ober, N. C. Maynard, M. R. Collier, D. J. McComas, N. F. Ness, C. W. Smith, and J. Watermann (2003), Predicting interplanetary magnetic field (IMF) propagation delay times using the minimum variance technique, J. Geophys. Res., 108 (A11026), doi:10.1029/2002JA009405.

Weimer, D. R. (2004), Correction to predicting interplanetary magnetic field (IMF) propagation delay times using the minimum variance technique, J. Geophys. Res., 109 (A12104), doi:10.1029/2004JA010691.

Wilcox, J. M. and N. F. Ness (1967), Sector Structure of the Quiet Interplanetary Magnetic Field, Science, 148 (3677),1592–1594, doi:10.1126/science.148.3677.1592.

Zhang, J., et al. (2007), Solar and interplanetary sources of major geomagnetic storms (Dst ≤ -100 nT) during 1996-2005, J. Geophys. Res., 112 (A10102), doi: 10.1029/2007JA012321.